MASTER'S THESIS

Transition zone influence on bridge dynamics using simplified loading conditions

Peter Nilsson

Master of Science in Engineering Technology
Civil Engineering

Luleå University of Technology
Department of Civil, Environmental and Natural Resources Engineering

LULEÅ UNIVERSITY OF TECHNOLOGY

LULEÅ UNIVERSITY OF TECHNOLOGY

TRANSITION ZONE INFLUENCE ON BRIDGE DYNAMICS USING SIMPLIFIED LOADING CONDITIONS

Peter Nilsson

Luleå University of Technology
Division of Structural Engineering

PREFACE

This project was initiated and carried out at Vectura consulting AB in Gothenburg during the period June – December of 2010. It is the final step for me towards a master of science degree in civil engineering at Luleå University of Technology.

I would like to take this opportunity to give my sincerest thanks to all the people that has helped me in any way during these years of studies.

Thanks to the staff at the division of structural engineering for great courses and always keeping an open door. Lars Bernspång, LTU shall especially be recognized for his great knowledge and open way of being.

Johan Jonsson, PhD, Vectura consulting AB, shall be thanked for shearing his great knowledge in the area of structural dynamics during this thesis. Tobias Larsson, PhD, Vectura consulting AB for great advice and guidance.

Last but definitely not least, thanks and love to all my family and friends.

Göteborg, December 2010

Peter Nilsson

ABSTRACT

In this work a stiffness transition zone between surrounding soil and a bridge structure is evaluated, showing how it affects the bridge dynamic behavior. It is made to give a better understanding of the transition zones impact on a bridge. A bridge structure is complex, depending on several interacting parts as soil-structure and rail-ballast. Simplifications are made in the work with the ground rule to simplify calculations but minimizing impact on basic structural behavior.

In principal the impact of a transitions zone has been studied by creating a representative model, verifying the model, performing a parametric study and then evaluation using design of experiment.

Limitations are made by using a 2-dimensional bridge in a single span, modeled linear elastic. The load is considered as a series of moving point loads.

The result shows that a transition zone impact the structures dynamic behavior. It is also shown that there exists a point where increasing the length of a transition zone gives no further positive contribution to the structure.

Within the scope of this thesis there has also been an investigation made on the topic of soil-structure interaction. This mainly on the fundamental property of eigen frequency. It is shown that surrounding soil of the modeled bridge decreases the first eigen frequency with respect to vertical deflections.

SAMMANFATTNING

I detta examensarbete undersöks om en styvhetsförändring i övergångszonen mellan mark och bro påverkar brons dynamiska beteende. Arbetet är initierat för att ge en bättre förståelse för hur styvheten i övergångszonen påverkar brons dynamiska beteende för åkande last. En brostruktur är komplex och består av ett flertal samverkande delar, så som bro-mark och räl-ballast. Förenklingar är gjorda i arbetet med en grundregel om att minimera påverkan på strukturens grundläggande beteende.

I princip har övergångszonens inverkan studerats genom att skapa en representativ modell, verifiera den, utföra en parameterstudie och sedan utvärdera dessa med statistisk försöksplanering.

Begränsningar är gjorda till en tvådimensionell bro i ett spann, linjärelastiskt modellerad. Lasten är beaktad genom en åkande punktlaster.

Resultatet visar att en linjär styvhetsförändring i övergångszonen påverkar de dynamiska responsparametrarna. Det visar även att en punkt existerar där ytterligare längre övergångszon inte påverkar strukturen.

Inom ramen för examensarbetet har också utförts en undersökning om hur omkringliggande mark påverkar brons egenfrekvenser. Det kan visas att omkringliggande mark sänker första egenfrekvensen med avseende på vertikal utböjning i detta studerade fall.

INDEX

NOTATIONS AND ABBREVATIONS

Explanations and units for notations and abbreviations.

Roman upper case

A	Amplitude	[m]
A	Cross sectional area	[m²]
A	Constant of integration	[m]
A_0	Initial amplitude	[m]
B	Constant of integration	[m]
$\boldsymbol{C}$	Damping matrix	[Ns/m]
D	Axle distance	[m]
E	Young's modulus	[N/m²]
F	Force	[N]
F_0	Force amplitude	[N]
G	Shear modulus	[Pa]
I	Second moment of inertia	[m⁴]
I	Impulse	[Ns]
$\boldsymbol{K}$	Stiffness matrix	[N/m]
M	Moment	[Nm]
$\boldsymbol{M}$	Mass matrix	[kg]
P	Concentrated force	[N]
V	Shear force	[N]
X	Steady-state displacement amplitude	[N]
X	Mode shape function	[m]

T	Transient solution	[-]
T	Natural period	[s]

Roman lower case

a	Constant of integration	[m]
a	Side width	[m]
a	Load propagation distance	[m]
a_i	Constant of integration	[m]
a_{max}	Maximum acceleration	[m/s^2]
c	Damping constant	[Ns/m]
c	Load velocity	[m/s]
c_l	Load velocity	[m/s]
c_s	Shear wave speed	[m/s]
c_cr	Critical damping	[Ns/m]
c_cr	Critical speed	[m/s]
$c_\mathrm{ray,soft}$	Rayleigh wave speed of soft medium	[m/s]
f	Natural frequency	[s^{-1}]
f	Distributed load	[N]
f_1	First natural frequency	[s^{-1}]
f_c	Calculation frequency	[s^{-1}]
f_det	Maximum detectable frequency	[s^{-1}]
f_eq	Equation frequency	[s^{-1}]
$f_{(\mathrm{j})}$	Natural frequency corresponding to the j-th mode of vibration	[s^{-1}]
l_e	Element size	[m]
m	Mass	[kg]
w	Deflection from undeformed plane	[m]
r	Damping ratio	[-]
t	Time coordinate	[s]
u	Displacement	[m]

u_0	Initial displacement	[m]
v	Velocity	[m/s]
v_0	Initial velocity	[m/s]
v_{cr}	Critical load velocity	[m/s]
w_0	Static displacement	[m]
x	Spatial coordinate	[m]

Greek upper case

Δt	Time increment	[s]

Greek lower case

α	Speed ratio	[-]
α	Mass proportional Rayleigh coefficient	[s^{-1}]
β	Damping ratio	[-]
β	Weighted natural frequency	[$s^{-1/2}$]
β	Stiffness proportional Rayleigh coefficient	[s]
β_i	Regression coefficient	[-]
δ	Dirac's delta function	[-]
ζ	Damping ratio	[-]
θ	Steady-state displacement phase shift	[-]
μ	Mass per unit length	[kg/m]
ρ	Density	[kg/m^3]
ω	Natural circular frequency	[s^{-1}]
ω_d	Damped natural circular frequency	[s^{-1}]
ω_{dr}	Driving circular frequency	[s^{-1}]
ω_b	Circular damping frequency	[s^{-1}]
$\omega_{(j)}$	Circular frequency corresponding to the j-th mode of vibration	[s^{-1}]
$\omega'_{(j)}$	Damped circular frequency	[s^{-1}]

Abbrevations

2D	2-Dimensional
3D	3-Dimensional
DAF	Dynamic amplification factor
DOF	Degree of freedom
FBD	Free Body Diagram
FE	Finite Element
FEM	Finite Element Model/Method
FFT	Fast Fourier Transform
MDOF	Multiple degree of freedom
PSD	Power Spectral Density
RMS	Root Mean Square
SDOF	Single degree of freedom

1 INTRODUCTION

In this section the reader will be introduced to the topic of this thesis.

1.1 Background

In the near future large developments will be done in the Swedish rail-road network. The main target at present is to build out bottle-necks but high-speed rail-road transportations is also a topic frequently discussed. Increasing train velocities place new demands on bridge structures. Transition zones play an important role in the total bridge structure, affecting a variety of parameters.

"Jump and bump" is a phenomenon known but not generally considered in current bridge design codes. As a train passes the transition zone and the abutment of a bridge it is given an upwards reaction force induced by stiffness discontinuity, velocity of the train and its weight. This creates a time period of low vertical contact forces as the train transfers further onto the bridge span, finally generating an impact-like impulsive load at a distance from the abutment. Increasing load speeds may amplify its effects.

1.2 Aim

The aim of this work is to investigate how a stiffness transition zone affects the dynamic behavior of a railway bridge structure. It is also to set the foundation for further studies on the subject. To improve the authors knowledge on the subject of structural dynamics and moving load Finite Element (FE) modeling is also a large portion of this project.

1.3 Limitations

The time available for this thesis was 20 weeks which induces limitations of the work possible to perform.

Loading

Loading of the structure has been done using a series of impulses. It is a set of concentrated loads placed on a path (set of nodes) having a triangular shaped time history. The loading property is pre-defined to a full extent before the analysis yielding no load – structure interaction. Thus this is a first study to a problem indicating the transition zones impact from an impulse loading perspective.

Portal frame

Only one portal frame railway bridge is considered with a ballasted track. This induces a result that doesn't span over all the existing bridge stock, but gives an indication of its impact.

All analyzes are conducted using a 2-dimensional (2D) model consisting of plane stress solid- and beam elements. Wave propagation is by nature 3-dimensional (3D). To make this kind of investigation it can be an idea to use a 2D model to draw more general conclusions.

The elastic deformations are assumed small in comparison to those of irreversible nature. Therefore linear elastic material properties are used.

Parametric study

To obtain conceptual efficiency (do to the time consuming analyses), terms of experiment methodology are used.

1.4 Outline

1. Introduction

Description of the problem, its background and main aims of the thesis.

2. Structural dynamics and theory

Short explanation of basic dynamic theories and studies of interest for the topic of this thesis.

3. Bridge geometry and materials

Introducing the materials and substructures contained in the main model.

4. FE model and numerical solution method

Explains how the FE-model represent the structure and what solution methods are used to solve the systems.

5. Model verification

Verifying the FE model with respect to convergence and energy dissipation.

6. Analysis

Description of the eigen-frequency and parametric analyzes.

7. Result and discussion

Results and evaluation of analysis.

8. Conclusions and further development.

Conclusions drawn from the work of the thesis and suggestions to further work on the subject.

2 STRUCTURAL DYNAMICS AND THEORY

Structural dynamics indicates the concept of structures subjected to time-varying loads inducing a time-varying response. A dynamic analysis is required when the inertia forces of a time-varying load give a significant impact on the structural response. There exist two model types:

- continuous models
- discrete-parameter models.

The distinction appears in the number of degrees of freedom (DOF). A discrete-parameter model contains a finite number of degrees of freedom. This number is infinite for the continuous model, demanding a closed form solution. Studying the single degree of freedom (SDOF) system gives insight in dynamic behavior and the equations are similar in matrix form for the multiple degree of freedom (MDOF) case.

2.1 Single degree of freedom system

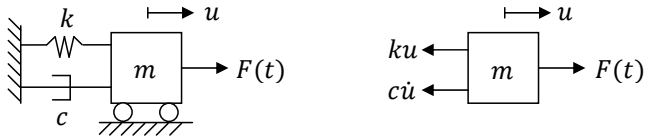

Figure (2.1) *Schematic (left) and free body diagram (right) of friction-free single degree of freedom system.*

Applying Newtons second law on the free body diagram in Figure (2.1) yields

$$m\ddot{u} + c\dot{u} + ku = F(x) \tag{2.1}$$

where:

m	mass	[kg]
c	damping constant	[Ns/m]
k	spring stiffness	[N/m]

F	force	[N]

Equation (2.1) is the equation of motion for the viscous damped spring – mass SDOF system.

2.2 Free vibration

When the system is not excited with an external force, $F = 0$, the motion is denoted as free vibration. The homogenous part of equation (2.1) describes this motion by

$$m\ddot{u} + c\dot{u} + ku = 0. \tag{2.2}$$

The undamped SDOF-system, $c = 0$ in equation (2.1), determines the systems circular frequency, ω, as

$$\omega = \sqrt{\frac{k}{m}}. \tag{2.3}$$

Circular frequency, ω and natural frequency, f is coupled by

$$\omega = 2\pi f. \tag{2.4}$$

Critical damping, c_{cr} is defined by the point where the solution of the characteristic equation corresponding to equation (2.2) is changing from real to complex roots. This point of damping gives the system a change in physical motion behavior. A system with damping less than the critical oscillates with an exponential decrease, apart from one with damping higher than the critical that strictly decrease exponentially. Critical damping is given as

$$c_{cr} = 2\sqrt{km} = 2m\omega. \tag{2.5}$$

Damping ratio, ζ is defined by

$$\zeta = \frac{c}{c_{cr}} = \frac{c}{2m\omega}. \tag{2.6}$$

The damped circular frequency, ω_d is given as

$$\omega_d = \omega\sqrt{1 - \zeta^2}. \tag{2.7}$$

A system with damping ratio $\zeta = 1$ is critically damped and gives the characteristic equation of equation (2.2) double roots. If $\zeta < 1$ the characteristic equation have complex roots and the system is called underdamped. $\zeta > 1$ yields real distinctive roots for the characteristic equation and the motion of the system is overdamped.

The displacement solution of the underdamped free vibration SDOF-system is given as

$$u(t) = Ae^{-\zeta\omega t}\sin(\omega_d t - \phi), \tag{2.8}$$

where the amplitude, A and the phase shift, ϕ are constants of integration, determined by initial conditions. The exponential term describes the decrease of energy in the system and the trigonometric term describes the oscillation. Figure (2.2) to Figure (2.4) displays the motion of the three different damping states for different initial conditions where $u(0) = u_0$ and $\dot{u}(0) = v_0$.

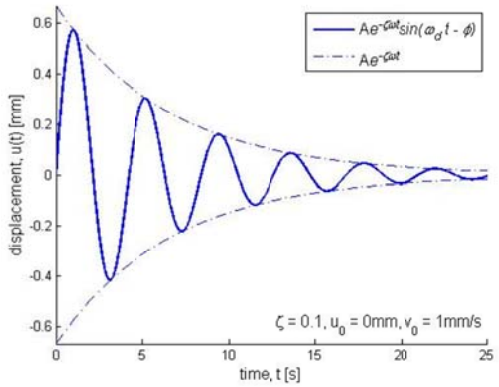

Figure (2.2) *Free vibration of an underdamped SDOF-system.*

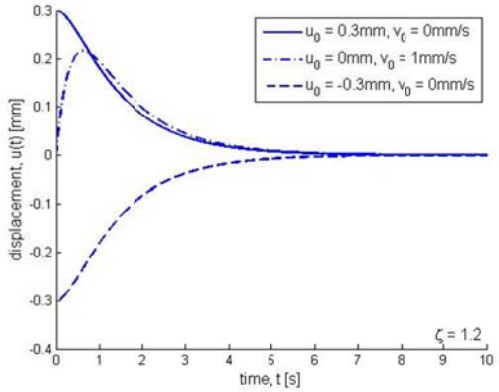

Figure (2.3) *Free vibration of an overdamped SDOF-system.*

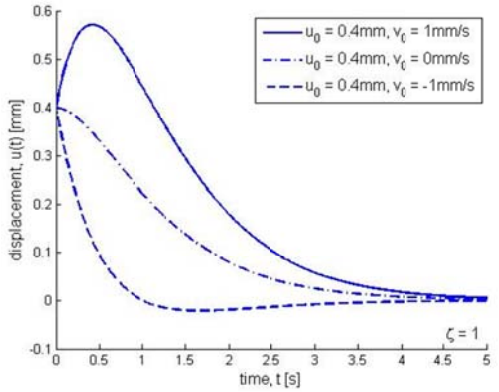

Figure (2.4) *Free vibration of a critically damped SDOF-system.*

2.3 Harmonic excitation

Harmonic excitation refers in this case to a sinusoidal single frequency force applied to the system. This force can for example be considered as

$$F(t) = F_0 \cos(\omega_{dr} t), \tag{2.9}$$

where:

F_0	force amplitude	[N]
ω_{dr}	driving circular frequency	[s^{-1}]

Inserting (2.9) into (2.1), yields

$$m\ddot{u} + c\dot{u} + ku = F_0 \cos(\omega_{dr} t). \tag{2.10}$$

This linear second order differential equation requires a homogenous solution according to equation (2.8). In the harmonic excited system the constants of integration of the homogenous solution are also dependent on the force amplitude, F_0 and the driving frequency, ω_{dr}. The homogenous solution is also denoted as transient response as it will fade out.

The particular solution, $u_p$can be written on the form

$$u_p = X cos(\omega_{dr} t - \theta) \tag{2.11}$$

where:

X	steady-state displacement amplitude	[N]
θ	steady-state displacement phase shift	[-]

This part of the solution is also called the steady-state response as it is the only substantial part when the transient response approaches zero.

Equation (2.8) and (2.11) now form the general response for the underdamped case excited by a harmonic load

$$u(t) = Ae^{-\zeta\omega t} \sin(\omega_d t - \phi) + X cos(\omega_{dr} t - \theta). \tag{2.12}$$

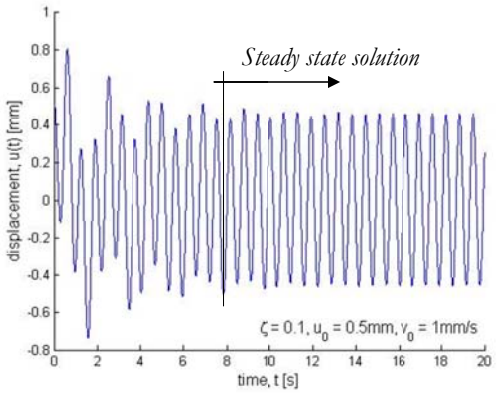

Figure (2.5) *Harmonically excited underdamped SDOF-system.*

The steady state displacement amplitude can be shown to be

$$X = \frac{f_0}{\sqrt{(\omega^2 - \omega_{dr}^2)^2 + (2\zeta\omega\omega_{dr})^2}} \tag{2.13}$$

where, $f_0 = \frac{F_0}{m}$ is the force amplitude per unit mass. Equation (2.13) can be rewritten to

$$\frac{X\omega^2}{f_0} = \frac{f_0}{\sqrt{(1-r^2)^2 + (2\zeta r)^2}} \tag{2.14}$$

where, $r = \frac{\omega_{dr}}{\omega}$ is the frequency ratio. This is for example shown in [3]. Equation (2.14) is a mathematical display of resonance. The steady-state displacement amplitude, X reaches its maximum value when exited with its natural frequency, $r = 1$, for all damping ratios, ζ. If the system only disperse low quantities of energy, $\zeta \to 0$, and is excited by a harmonic load with driving frequency equal to the natural frequency, the amplitude grows towards infinity. Equation (2.14) is evaluated graphically in Figure (2.6).

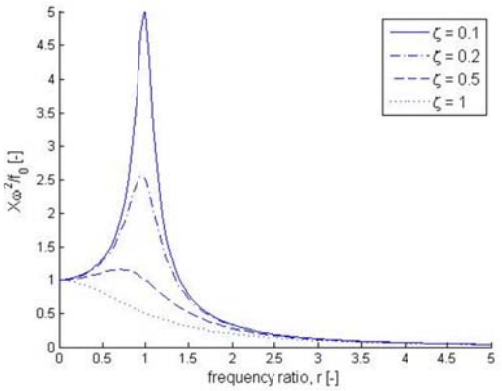

Figure (2.6) *Illustration of resonance expressed in steady state displacement.*

2.4 Impulse loads

Impulsive loads is assumed to play an important role to the "jump and bump".

The response of a system subjected to an impulsive load is identical to its response of certain initial condition, if the impulse is very short. An impulse can be described as

$$F(t) = \begin{cases} 0 & t \in (-\infty, \tau - \varepsilon] \\ \frac{F*}{2\varepsilon} & t \in (\tau - \varepsilon, \tau + \varepsilon), \\ 0 & t \in [\tau + \varepsilon, \infty) \end{cases} \tag{2.15}$$

where ε is small. Equation (2.15) is exhibited as a graph in Figure (2.7). The impulse load is defined by

$$I(\varepsilon) = \int_{\tau-\varepsilon}^{\tau+\varepsilon} F(t)dt = F*. \tag{2.16}$$

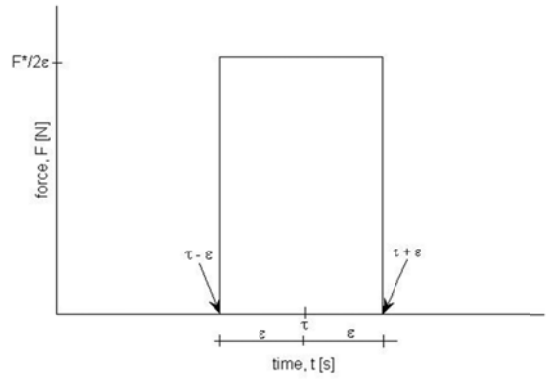

Figure (2.7) *Time history of a rectangular impulse.*

The response of a single degree of freedom system to an impulse load can be described by the solution of free vibration with the initial conditions

$$u_0 = 0, v_0 = \frac{F*}{m}. \tag{2.17}$$

This yields the dynamic displacement for the underdamped case

$$u(t) = \frac{F*}{m\omega_d} e^{-\zeta\omega t} sin\omega_d t. \tag{2.18}$$

If the form of the impulse is known, it can be solved explicitly as a non-homogenous second order differential equation, described by eq. (2.1). It is needed to be solved in two phases, one during and one after the load appliance. The result of these impulses can be plotted in terms of the dynamic amplification factor, (DAF), as a function of the load duration, t_1, for various impulse shapes. See Figure (2.8). DAF is the ratio of maximum dynamic displacement and static displacement.

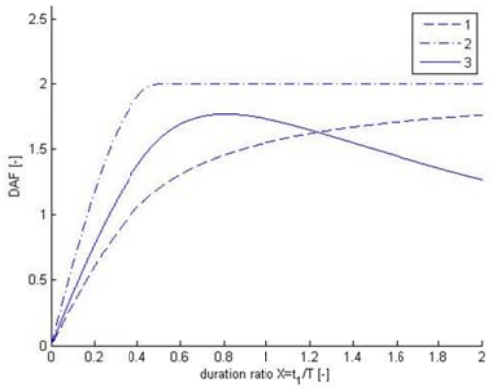

Figure (2.8) *Impulse response spectra. Dynamic amplification factor of SDOF system subjected to various formed impulse loads, 1. rectangular, 2. suddenly applied triangular, 3. sine formed.*

Derivations of the DAFs are shown in appendix A.

2.5 Bending vibration of a beam

The bending vibration of a beam has been studied to gain fundamental understanding of bridge behavior. A infinitesimal element from an Euler-Bernulli beam loaded with a distributed load is displayed in the FBD below.

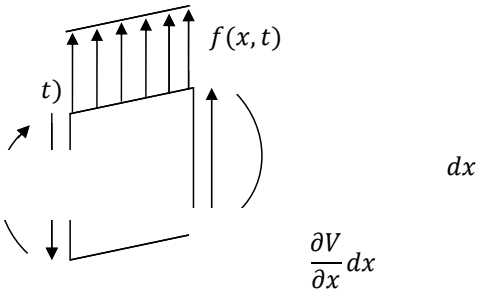

Figure (2.9) *FBD of Euler-Bernulli beam element excited with distributed load.*

Applying Newtons second law of motion on the forces acting on the body one can excecute the general equation of motion for the undamped Euler-Bernulli beam as

$$\rho A(x)\frac{\partial^2 w(x,t)}{\partial t^2}+\frac{\partial^2}{\partial x^2}\left[EI(x)\frac{\partial^2 w(x,t)}{\partial x^2}\right]=f(x,t) \tag{2.19}$$

where:

t	time coordinate	[s]
x	spatial coordinate	[m]
ρ	density	[kg/m^3]
A	cross sectional area	[m^2]
w	deflection from undeformed plane	[m]
E	Young's modulus	[N/m^2]
I	second moment of inertia	[m^2]

This equation can be solved using a separation-of-variables technique based on the assumption that the deflection can be written as a product on the form,

$$w(x,t) = X(x)T(t), \tag{2.20}$$

where the spatial solution, $X(x)$ is decided by the homogenous part of the general solution. The spatial part is also the eigen-functions of the analytical solution called mode-shapes or modal shape functions. Each of the mode-shapes are coupled with an eigen value, a natural frequency. The spatial solution can be shown to have the general form

$$X(x) = a_1 sin\beta x + a_2 cos\beta x + a_3 sinh\beta x + a_4 cosh\beta x. \tag{2.21}$$

Equation (2.21) consists of four unknown constants of integration, a_i and the constant β. Four of these unknowns are solved with boundary conditions and the last one is combined with constants of integration from the temporal solution, $T(t)$.

The general solution of the temporal part yields

$$T(t) = Asin\omega t + Bcos\omega t. \tag{2.22}$$

Applying boundary conditions on the trigonometric spatial solution one can realize it has an infinite number of solutions. Summation of this infinite series of solutions will generate the general solution for free undamped vibration

$$w(x,t) = \sum_{n=1}^{\infty}(A_n sin\omega t + B_n cos\omega t)X_n(n). \tag{2.23}$$

For execution of this modal solution the mode-shape functions need to satisfy the orthogonality property

$$\int_0^l X_n(x)X_m(x)dx = 0 \tag{2.24}$$

where l is the length of the beam and $n \neq m$.

2.6 Dynamic response of a beam exited by a moving load

Vehicles using bridges are in motion. This implies that both moving loads and dynamic response needs to be considered.

Analytic and semi-empirical solutions of dynamic response of continuous systems are derived by Ladislav Fryba in *Vibrations of solids and structures subjected to moving loads* [1].

The case of a simply supported beam will be discussed breifly here.

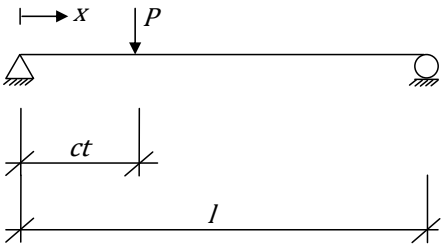

Figure (2.10) *Schematic of a simply supported beam subjected to a moving load.*

The system complies under the following assumptions:

- Euler-Bernulli beam theory assumptions are valid.
- Damping is proportional to the velocity of the beam, vicious damping.
- Constant moving load has a fix speed.
- Beam stiffness is constant over the length.
- Mass of the load is small compared to the mass of the beam.

Applying these assumptions, the system can be described with the equation of motion

$$EI\frac{\partial w^4(x,t)}{\partial x^4} + \mu\frac{\partial w^2(x,t)}{\partial t^2} + 2\mu\omega_b\frac{\partial w^2(x,t)}{\partial t^2} = \delta(x-ct)P. \tag{2.25}$$

The boundary conditions of the simply supported case are

$$w(x,t)|_{x=0} = w(x,t)|_{x=l} = \left.\frac{\partial w^2(x,t)}{\partial x^2}\right|_{x=0} = \left.\frac{\partial w^2(x,t)}{\partial x^2}\right|_{x=l} = 0, \tag{2.26}$$

and the initial conditions for initially rest

$$w(x,t)|_{t=0} = \left.\frac{\partial w(x,t)}{\partial t}\right|_{t=0} = 0 \tag{2.27}$$

where:

w	vertical deflection from undeformed plane	[m]

E	Young's modulus of elasticity	[N/m²]
I	second moment of inertia	[m²]
μ	constant mass per unit length	[kg/m]
ω_b	circular damping frequency	[s⁻¹]
P	constant concentrated force	[N]
c	constant load velocity	[m/s]
x	spatial coordinate	[m]
t	time coordinate	[s]
δ	Dirac's delta function	[-]

Equation (2.25) with initial and boundary conditions, (2.26) and (2.27) can be solved using integral transformations. This yields the solution for a light damped case on the form of an infinite series

$$w(x,t) = w_0 \sum_{j=1}^{\infty} \left\{ \begin{array}{l} \frac{1}{j^2[j^2(j^2-\propto^2)^2+4\propto^2\beta^2]}[j^2(j^2-\propto^2)\sin j\omega t - \\ \frac{j\propto[j^2(j^2-\propto^2)-2\beta^2]}{\sqrt{j^4-\beta^2}} e^{-\omega_b t}\sin\omega'_{(j)}t - \\ 2j\alpha\beta(cosj\omega t - e^{-\omega_b t}cos\omega'_{(j)}t)]sin\frac{j\pi x}{l} \end{array} \right\}. \quad (2.28)$$

where:

w_0	static displacement at $x = l/2$ when the concentrated load is applied at the same point	[m]
α	c/c_{cr} , speed ratio	[-]
c_{cr}	$2f_{(j)}l/j$, critical speed	[m/s]
$f_{(j)}$	natural frequency corresponding to the j-th mode of vibration	[s⁻¹]
$\omega_{(j)}$	circular frequency corresponding to the j-th mode of vibration	[s⁻¹]
$\omega'_{(j)}$	$\left(\omega_{(j)}{}^2 - \omega_b^2\right)^{1/2}$, circular frequency of the damped case with light damping	[s⁻¹]
β	$\omega_b/\omega_{(j)}$, damping ratio	[-]

Equation (2.28) can be visualized with the graph of $w(l/2,t)/w_0$ as a function of

ct/l, i.e. the dynamic/static deflection ratio as a function of load position. Figure (2.11) shows the case of no damping, $\beta = 0$.

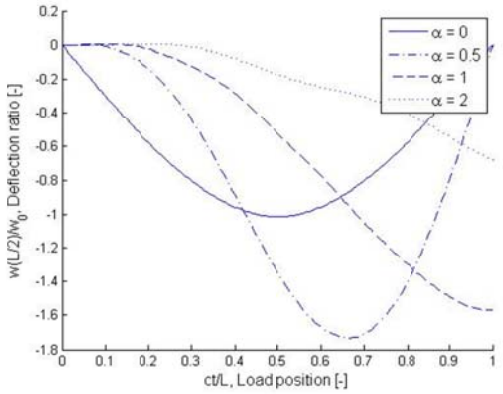

Figure (2.11) *Deflection ratio at* $x = l/2$ *as a function of load position.*

2.7 Rayleigh waves, wave propagation and element size

The Rayleigh wave is a wave created along a free surface. It is a combination of longitudinal and transversal waves creating an elliptic particle motion. The wave propagation speed is slightly lower than for the shear wave (s-wave) given by

$$c_s = \sqrt{\frac{G}{\rho}} \tag{2.29}$$

The relationship between shear wave speed and Rayleigh wave speed is shown in Figure (2.12) as a function of Poisson's ratio.

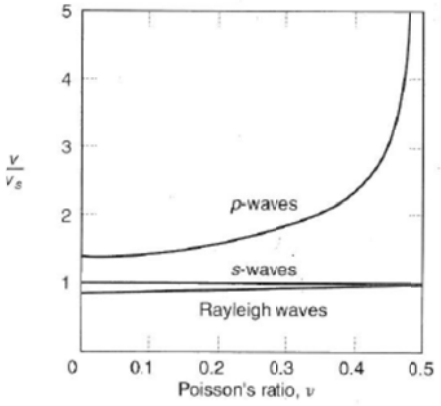

Figure (2.12) *Ralationship between wave speed ratio and Poisson´s ratio,* v_s *is shear wave speed, figure from* [12].

When determining the element size of the mesh in the numerical FE-models one shall fit 6-8 elements on the shortest wavelength considered. Young's modulus of the soil can also be determined from the propagating shear wave speed. Shear wave speed in an elastic material is given by (2.29) and the relation between the elastic and shear modulus is

$$G = \frac{E}{2(1+\nu)}. \tag{2.30}$$

Inserting eq. (2.30) in (2.29) yields

$$E = 2\rho(1+\nu){c_s}^2 . \tag{2.31}$$

Thus by knowing the shear wave speed, the modulus of elasticity is easily determined. The shear-wave length, l_s is given by

$$l_s = \frac{c_s}{f}, \tag{2.32}$$

where, f is the frequency of oscillation. Under the assumption of eight elements the maximum allowed element size is given as

$$l_e = \frac{c_s}{8f}. \tag{2.33}$$

2.8 Moving load on an elastic half-space

Ballast and subballast are unbound non-cohesive granular material that gain small permanent deformations compared to the reversible deformations. This is why they can be modeled as linear elastic continuums [2]. Cumulative effects of permanent deformations are though of great importance for topics not discussed in this thesis. In [2] a study is made in the following main steps:

- A constant moving load on an elastic half-space is modeled numerically and compared with corresponding analytical methods of [2], mainly to confirm the model.
- A constant moving load is passing a stiffness discontinuity between a soft and a stiff material.
- Influence of the length of a stiffness transition between the two materials is investigated.

Schematic of the model in the first step is displayed in Figure (2.13).

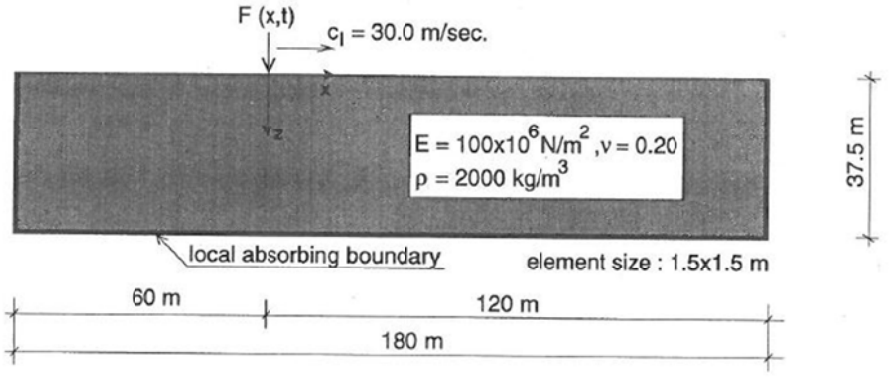

Figure (2.13) *Schematic of load model, figure from* [2].

When the load instantaneously reaches its velocity, it induces two Rayleigh waves. One propagates in the direction of the load and one in the opposite direction. These waves are marked (R+) and (R-) in Figure (2.14)

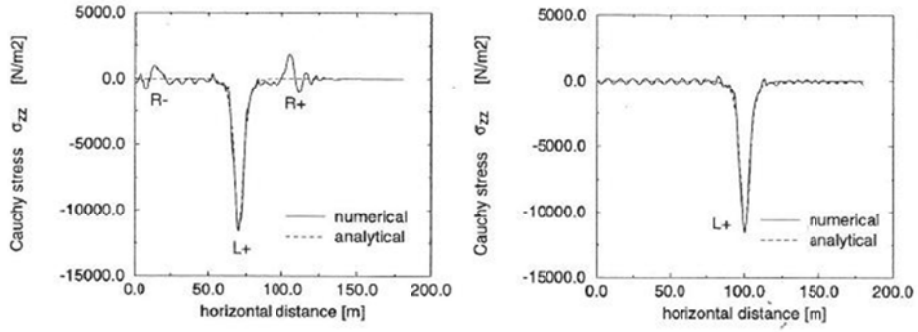

Figure (2.14) *Vertical stress after 10 and 40m load propagation at a vertical distance from the surface of 5.68m, figure from* [2].

To consider that the structure is semi-infinite a local absorbing boundary is modeled and good correspondence to analytical results is achieved.

The second step is made with schematic according to Figure (2.15).

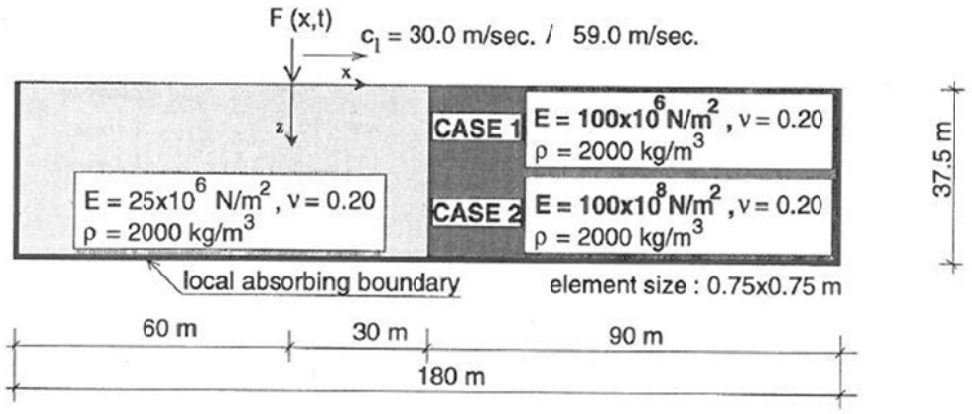

Figure (2.15) *Schematic of load model considering a stiffness discontinuity, figure from* [2].

Case I according to Figure (2.15) is first and mainly considered. Again when the load starts to move it induces two Rayleigh-waves. When the Rayleigh-wave reaches the stiffness discontinuity it refracts into the new and stiffer medium. Partly it also reflects back in the direction opposite of the load. As the load passes the stiffness discontinuity it generates another Rayleigh-wave, one part refracts into the second material and another part reflects back.

In Figure (2.16) the following notations are used:

$R1\_$ Start motion induced Rayleigh-wave in negative load propagation direction.

$R1_{refr+}$ Refracted part of the start-motion induced Rayleigh wave.

$R1_{refl-}$ Reflected part of the start-motion induced Rayleigh wave.

L_+ Steady-state response

$R2_{refr+}$ Refracted part of the Rayleigh-wave induced by the motion over stiffness discontinuity.

$R2_{refl-}$ Refected part of the Rayleigh-wave induced by the motion over stiffness discontinuity.

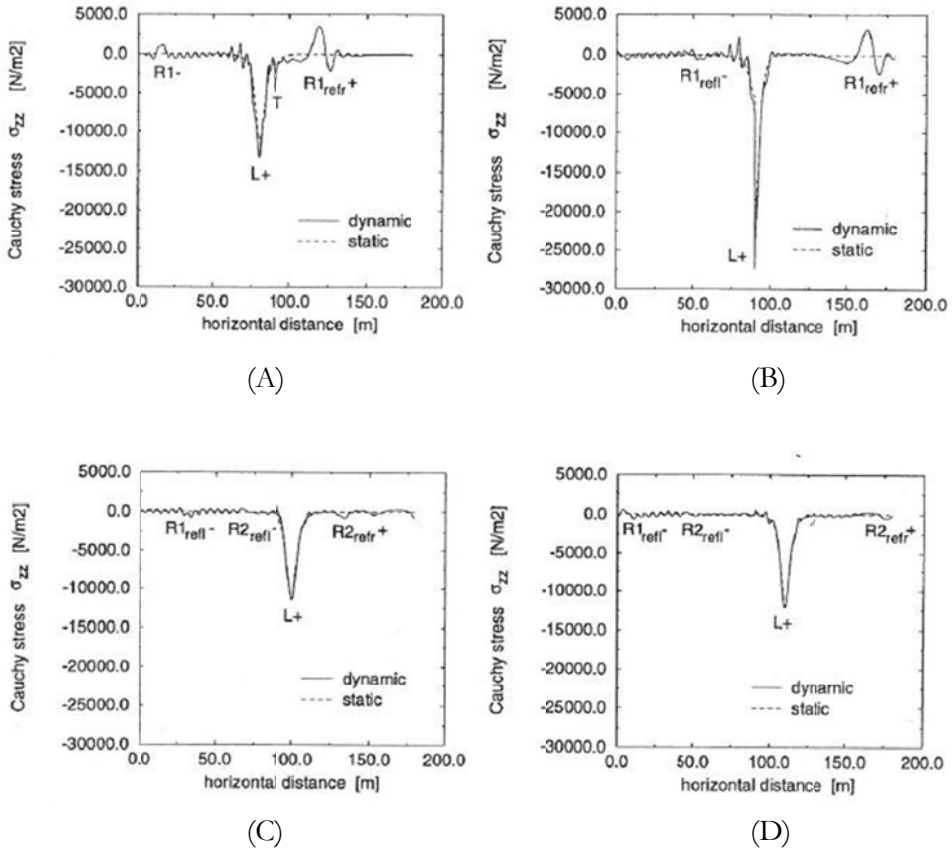

Figure (2.16) *Vertical stresses at 5.84m distance from surface,* $c_l/c_{ray,soft\ medium}$*, figure from* [2].

(A) – 20m load propagation

(B) – 30m load propagation

(C) – 40m load propagation

(D) – 50m load propagation.

The dynamic amplification factor, DAF, are calculated in [2] dependent of the following factors

c_l	Load propagation speed	[m/s]
$c_{ray,soft\ medium}$	Rayleigh wave speed in the first softer medium	[m/s]
a	Load propagation distance	[m]

Table (2.1) *DAF for different speeds and propagation distances.*

a	$c_l/c_{ray,soft}$	DAF
20	0.46	1.21
30	0.46	1.30
50	0.46	1.07
20	0.90	2.51
30	0.90	5.66
50	0.90	1.09

When the load has propagated past the stiffness discontinuity the DAF decreases as an effect of the new and higher Rayleigh wave speed. In the case of higher load speed the DAF is of a larger magnitude as the Rayleigh wave and the steady state response interact. It can also be noted that when the two positive propagating refracted Rayleigh waves interact at $c_l/c_{ray,soft\ medium}$ =0.9 they are of larger stress magnitude then the steady-state response. The large DAF of 30m load propagation is partly due to compatibility requirements (material splice).

In the third part of [2] a transition zone is introduced with schematic and results on the form of DAF according to Figure (2.17) and Figure (2.18).

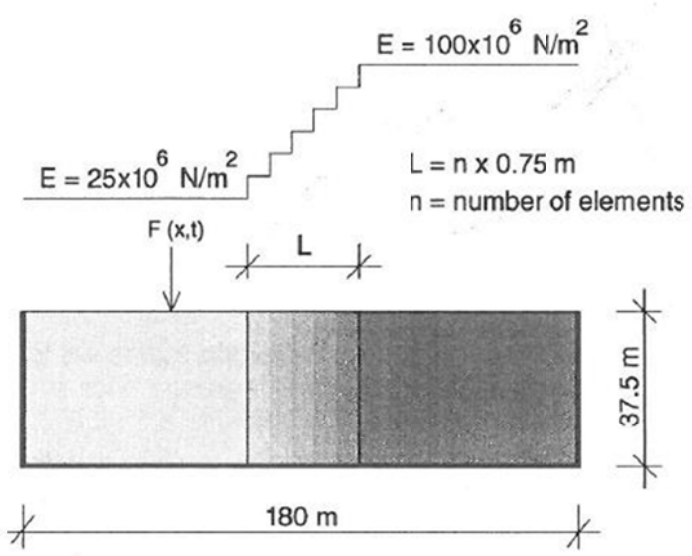

Figure (2.17) *Schematic of the modeled elastic half-space with transition zone, figure from* [2].

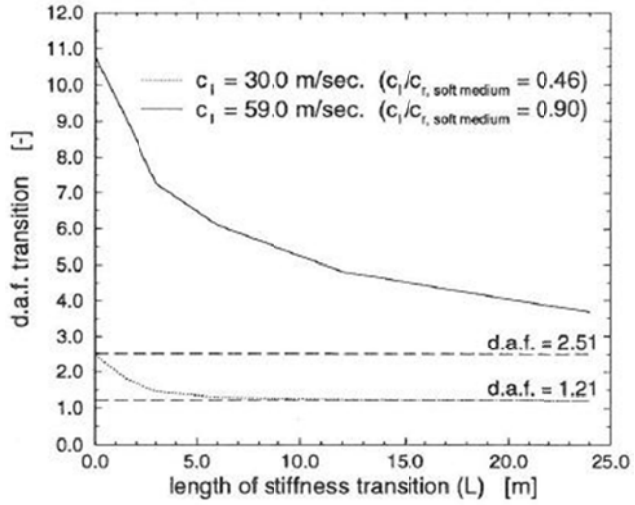

Figure (2.18) *DAF as a function of transition zone length, figure from* [2].

One can easily see the connection between DAF and transition zone length. Even though ballast and rail, placed over the discontinuity, will be elements that decrease these effects, they are still of great importance [2].

2.9 Sampling theorem

There exists a sampling theorem, stated for example in [13], given by

$$\omega_{max} = \frac{\omega_s}{2} = \frac{1}{2}\left(\frac{2\pi N}{T}\right) \tag{2.34}$$

where:

ω_{max}	maximum detectable frequency (Nyquist frequency)	[s^{-1}]
ω_s	sampling frequency	[s^{-1}]
N	number of samples	[-]
T	sample length	[s]

Thus, the maximum detectable frequency is half of the sampling frequency. As an effect of aliasing, only 80% of the Nyquist frequency is recommended to be considered as confirmed in practice [13].

Thus, if the signal that shall be evaluated consist of frequencies higher than 40% of the sampling frequency, filtering of the signal shall be adapted.

2.10 Rayleigh damping

Rayleigh damping or proportional damping is a way of introducing vicious damping to a structural system. Rayleigh damping will be used throughout this work. Rayleigh damping assumes a damping matrix proportional to a combination of stiffness and mass by

$$\boldsymbol{C} = \alpha \boldsymbol{M} + \beta \boldsymbol{K}. \tag{2.35}$$

Damping ratio, ζ, for mode i is given as

$$\zeta_i = \frac{1}{2}\left[\alpha \frac{1}{\omega_i} + \beta \omega_i\right]. \tag{2.36}$$

Two separate modes i and j defined by the same proportional Rayleigh constants yields

$$\alpha = \frac{2\omega_i \omega_j (\zeta_j \omega_i - \zeta_i \omega_j)}{\omega_i^2 - \omega_j^2} \tag{2.37a}$$

$$\beta = \frac{2(\zeta_i \omega_i - \zeta_j \omega_j)}{\omega_i^2 - \omega_j^2}. \tag{2.37b}$$

In Figure (2.19) a typical Rayleigh damping distribution is visualized. Thus from knowing two specific damping ratios of two frequencies, damping over all frequencies is applied. Knowing the contained frequency interval of the signal and Rayleigh damping constants of the structure, one has control of the damping.

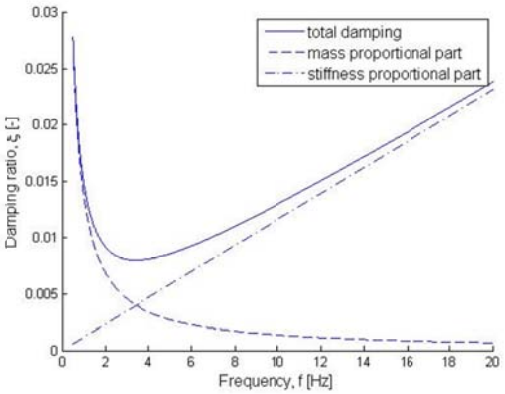

Figure (2.19) *Rayleigh damping.*

2.11 Fourier transform and Power Spectral Density (PSD)

Fourier transforms considers the concept of signal transformation. In the case of structural dynamics, the transform between time and frequency domain is of great importance. This concept was first presented by Jean-Baptiste Joseph Fourier

(1768-1830) and states that every random signal can be presented as a sum of orthogonal trigonometric functions.

Power Spectral Density (PSD) is a frequency domain representation of arbitrary vibration signal. It filters out separate trigonometric signals and evaluates its average intensity, the Root-Mean-Square (RMS) parameter. This intensity is coupled with a specific frequency. Thus, the intensity, can be plotted as a function of vibration frequency, a PSD-plot. RMS is defined by

$$RMS = \sqrt{\lim_{T\to\infty} \frac{1}{T} \int_{-T/2}^{T/2} x^2(t)dt}, \tag{2.38}$$

where

T	natural period	[s]
$x(t)$	time signal.	[valid magnitude]

3 BRIDGE GEOMETRY AND MATERIALS

In the modeled structure all geometric and material parameters used are based upon design codes and realistic values. They are not from a specific construction. The two dimensional model is calculated with a depth of 6m. This is an approximate used width of a single track railway bridge.

3.1 Geometry

The bridge considered is a concrete portal frame bridge with a single span of 15.8m. It has a slab thickness of 500mm and a width of 6m. The frame legs are 700mm thick and 6.4m high.

Ballast and sub-ballast are assumed to be of the same thickness, 400mm. They differ in geometrical proportions, which is adjusted with the density. This affects the dynamical properties of the ballast bed, but the simplifications are needed when modeling in 2D.

Surrounding soil is assumed to be a semi-infinite halfspace.

Figure (3.1) *Sketch of the bridge modeled.*

1. UIC60 Rail

2. Ballast bed, 2x400mm, ballast and sub-ballast

3. Surrounding soil, 20m in horisontal direction from frame legs, 3m depth from foundation.

4. Transition zone, varying in length and stiffness, 1m depth.

5. Frame bridge legs, 700mm thick, 6800mm high.

6. Foundations, 1000mm thick, 2000mm wide.

7. Bridge deck, 500mm thick, span width 15800mm.

3.2 Materials and sub parts geometry

Material properties are collected from the literature and presented below.

3.2.1 Concrete

C30/37 quality is assumed. The Young's modulus is increased by 10% to represent dynamic behavior. Parts consisting of concrete are the sleepers and the bridge frame structure (object 7 and 8 of Figure (3.1)). These data are chosen in accordance with [5].

Table (3.1) *Concrete material properties.*

Notation	Parameter	Value	Unit
ν	Poisson's ratio	0.2	[-]
ρ	Density	2500	[kg/m³]
E	Young's modulus	36.3	[GPa]

3.2.2 Steel

Steel properties are chosen according to [6] and is presented in Table (3.2).

Table (3.2) *Steel material proporties.*

Notation	Parameter	Value	Unit
ν	Poisson's ratio	0.3	[-]
ρ	Density	7800	[kg/m³]
E	Young's modulus	210	[GPa]

The rail is the only considered steel part, see object 1 Figure (3.1) and is of UIC60 type. Cross section properties are found in Table (3.3). The rail geometry is shown in Figure (3.2).

Table (3.3) *UIC 60 cross section parameters.*

Notation	Parameter	Value	Unit
A	Cross section area	7687	[mm²]
I_{xx}	Cross sectional moment of inertia	3055	[cm⁴]

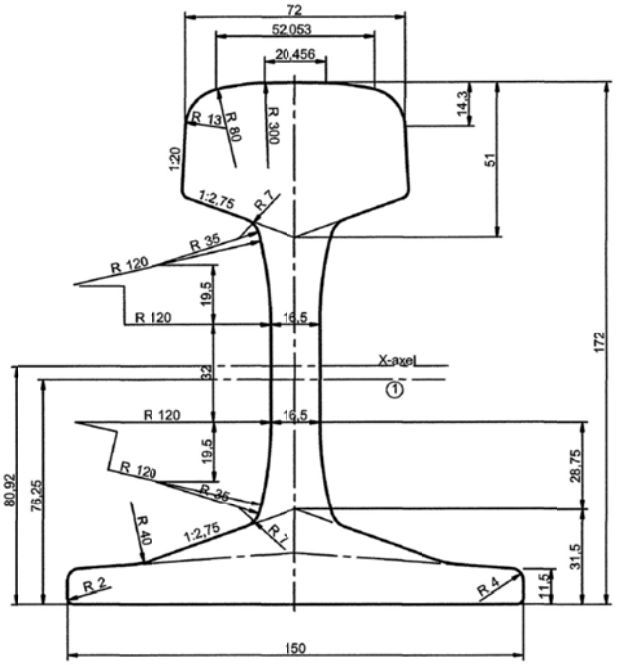

Figure (3.2) *UIC60 Cross section, figure from* [14]

For simplification, an equivalent square cross section is used, see Table (3.4).

Table (3.4) *Rail equivalent cross section parameters.*

Notation	Parameter	Value	Unit
a	Side width	165	[mm]
ρ	Density	4425	[kg/m³]

3.2.3 Surrounding soil

Surrounding soil is marked as object 3 in Figure (3.1). The structure is assumed to be surrounded by material of properties the same as sub-ballast. According to [7], the shear wave speed of a moraine material varies between 200 and 700m/s where the lowest wave-speed is used. Material parameters for the surrounding soil are shown in Table (3.5).

Table (3.5) *Soil material parameters.*

Notation	Parameter	Value	Unit
ν	Poisson's ratio	0.1	[-]
ρ	Density	1900	[kg/m³]
E	Young's modulus	167	[MPa]

Soil parameters other than the Young's modulus are collected from [8].

3.2.4 Ballast

Geometry of the bridge ballast-bed is given by Figure (3.3). Corresponding material properties are given by Table (3.6) and Table (3.7).

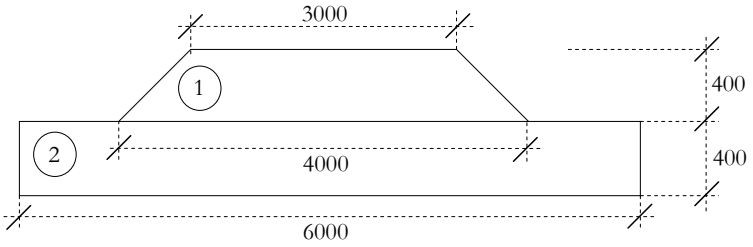

Figure (3.3) *Sketch of assumed ballast bed.*
1. Ballast, 2. Sub-ballast.

Table (3.6) *Ballast material properties.*

Notation	Parameter	Value	Unit
ν	Poisson's ratio	0.1	[-]
ρ	Density	1700	[kg/m³]
E	Young's modulus	150	[MPa]

Table (3.7) *Sub-ballast material properties.*

Notation	Parameter	Value	Unit
ν	Poisson's ratio	0.1	[-]
ρ	Density	1900	[kg/m³]
E	Young's modulus	167	[MPa]

To account for the geometrical differences of the ballast and the sub-ballast when using a plane model, the ballast density is modified. Included in the ballast density is the weight of the sleepers, 250 kg, placed with a 600 mm spacing.

$$\rho_{mod.bal} = \rho_{bal}\frac{A_{bal}}{A_{mod.bal}} + \frac{m_{sl}}{cc_{sl}\,A_{mod.bal}}$$
$$= 1700\ \frac{kg}{m^3} \times \frac{3.5m \times 0.4m}{6m \times 0.4m} + \frac{250kg}{0.6m \times 6m \times 0.4m} \sim 1170\,\frac{kg}{m^3}. \quad (3.1)$$

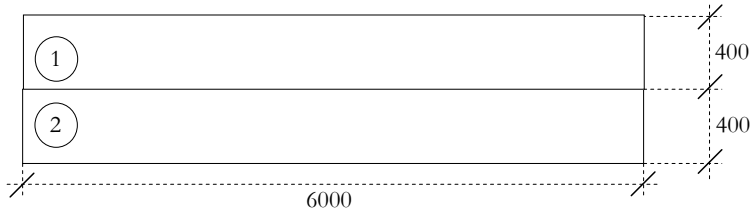

Figure (3.4) *Sketch of ballast bed with equivalent parameters.*
1. Ballast, 2. Sub-ballast.

3.2.5 Transition zone

The transition zone is assumed to have a graded stiffness, see Figure (3.5), and a depth of 1m. The length of one stiffness slice, L_e , varies between 0.2 and 0.8m. Material properties apart from the Young's modulus is equivalent with the sub-ballast described above. The Young's modulus changes linearly from the soil value towards specific end stiffness.

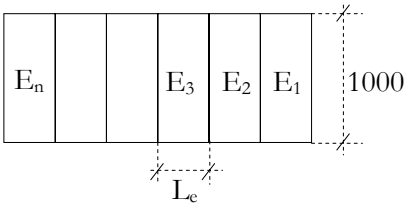

Figure (3.5) *Principal sketch of the transition zone composition.*

3.3 Damping

Rayleigh damping is applied to all materials in the model. Damping properties is taken from [9] and is presented in Table (3.8). The surrounding soil, ballast, sub-

ballast and the stiffness transition, shear damping properties, denoted as soil in Table (3.8).

Table (3.8) *Material damping properties.*

Material	ζ_i [%]	f_i [Hz]	ζ_i[%]	f_i [Hz]	α [s^{-1}]	β [s]
Steel	0.08	4.86	0.2	17.08	0.0152	$3.60734 \cdot 10^{-5}$
Concrete	2.75	3.63	1.16	17.82	1.1963	$1.1178 \cdot 10^{-4}$
Soil	0.8	3	1.5	12	0.1709	$3.6782 \cdot 10^{-4}$

Using the modal damping ratio and corresponding frequency in Table (3.8) the mass and stiffness proportional constants α and β can be calculated. Figure (3.6) through Figure (3.8) show the relative damping as a function of frequency for the used materials.

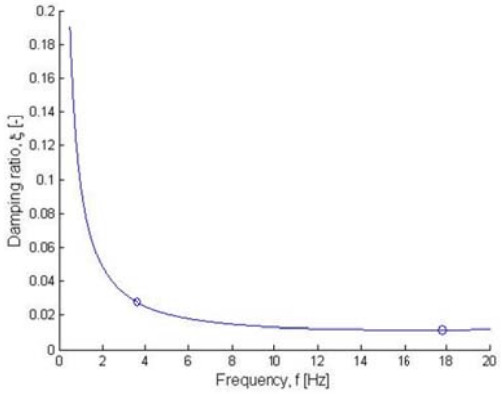

Figure (3.6) *Concrete damping distribution.*

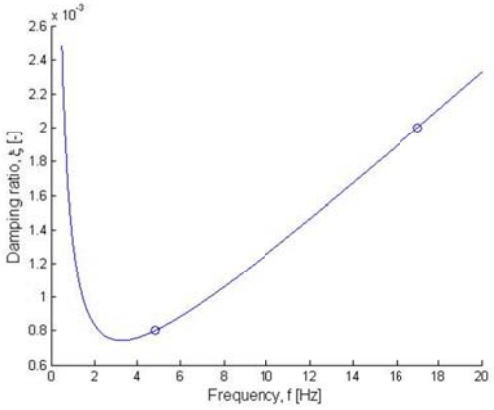

Figure (3.7) *Steel damping distribution.*

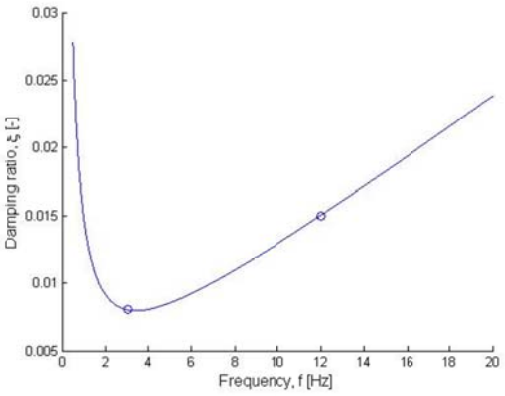

Figure (3.8) *Soil damping distribution.*

4 FE-MODEL AND NUMERICAL SOLUTION METHOD

The 2D model in this thesis is a combination of beam- and solid elements. Modeling is carried out with the software *BRIGADE* which uses an *ABAQUS* base.

4.1 Sub parts of main model

The numerical model is built up by a number of sub parts and later assembled. Elements used in the models are listed in Table (4.1). Figure (4.1) and Figure (4.2) show the geometric assembly and the mesh of the structure.

Table (4.1) *Element types.*

Sub-part	Type	Analysis name
Surrounding soil	4-node solid planar element	CPS4
Ballast	4-node solid planar element	CPS4
Sub-ballast	4-node solid planar element	CPS4
Rail	2 node Timoshenko beam element	B21
Portal frame	2-node Timoshenko beam element	B21
Semi infinite part	4-node semi infinite element	CINPS4
Foundations	4-node solid planar element	CPS4

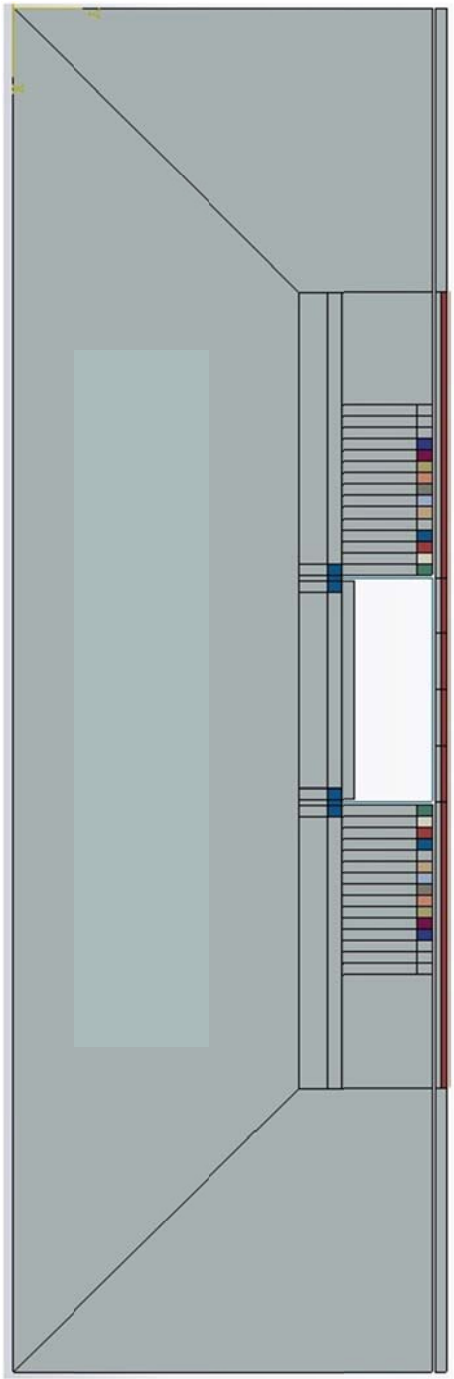

Figure (4.1) *Geometric assembly of modeled bridge. Different colors correspond to different material properties*

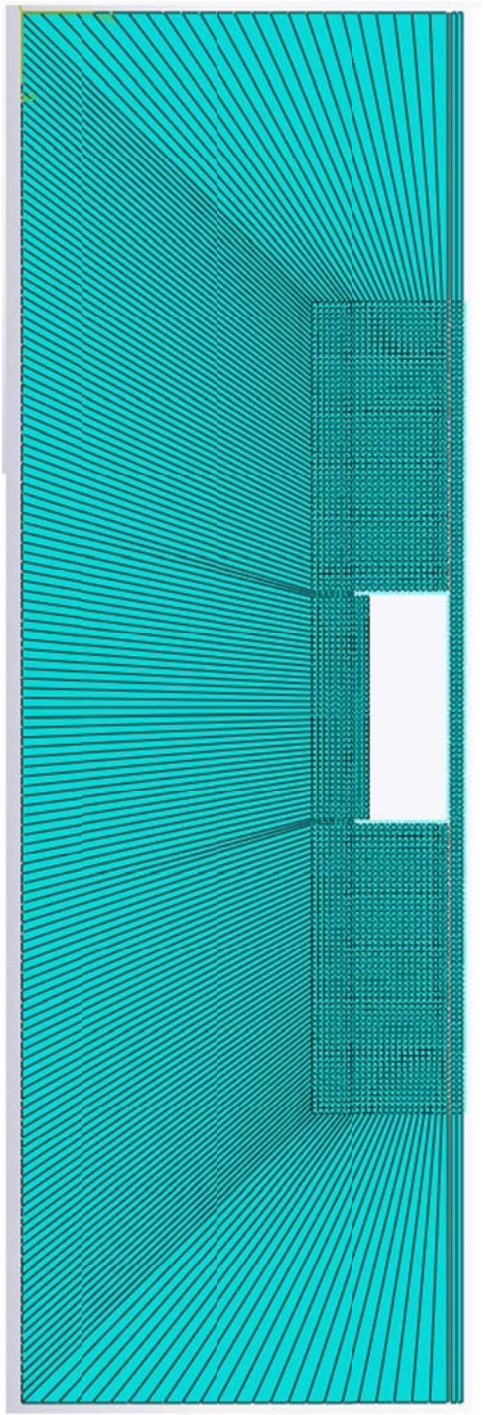

Figure (4.2) *Meshed model, 0.4m element size. Note the boundary elements that are used to simulate a semi- infinite half space.*

4.2 Loads

4.2.1 Dynamic live load

The train load is modeled by a series of impulses according to Figure (4.3) and Figure (4.4).

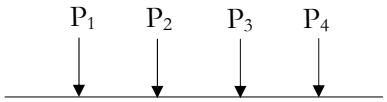

Figure (4.3) *Spatial position of the loads.*

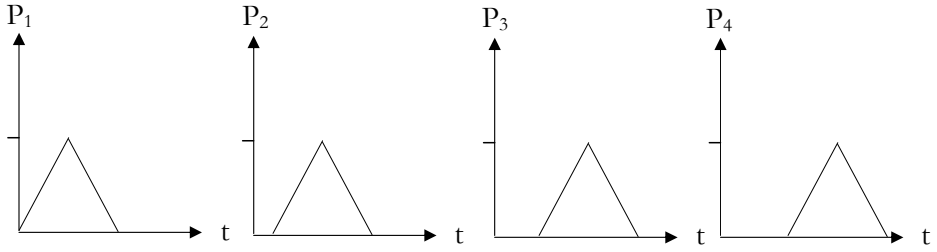

Figure (4.4) *Duration and time position of each load.*

4.2.2 HSLM A1

As train load the HSLM-A1 [10] has been used with axle loading according to Figure (4.5) and Table (4.2).

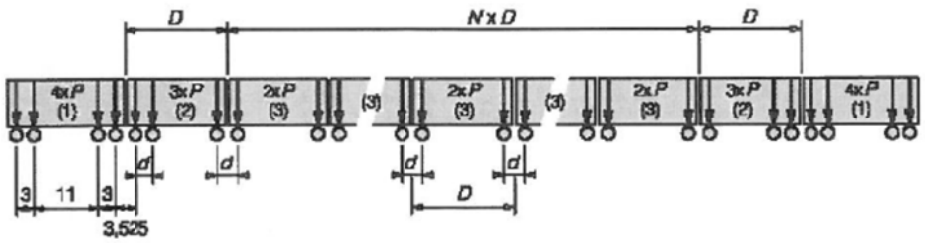

Figure (4.5) *Principal sketch of HSLM A1 from* [10]. *(1) Engine carriage, (2) coach connected to engine carriage, (3) intermediate carriage.*

Table (4.2) *HSLM-A1 Parameters of* Figure (4.5)

Notation	Parameter	Magnitude	Unit
N	No. of intermediate coaches	18	[-]
D	Length of an intermediate coach	18	[m]
d	Distance within boggie	2	[m]
P	Load	170	[kN]

4.2.3 Harmonic load with frequency interval

To examine the dynamic properties of the bridge structure, harmonic excitation was used. A frequency sweep was created using MATLAB, see APPENDIX 0. Part of the load-signal is displayed in Figure (4.6). Used frequency interval is from 0.1-30 Hz, increasing 0.1Hz each step.

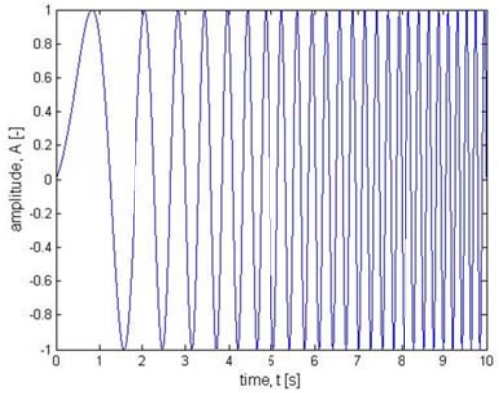

Figure (4.6) *Time history of the used frequency sweep, 0.1-30Hz.*

4.2.4 Stationary harmonic load

Harmonic excitation was used in the convergence study of the numerical model. The harmonic load used was

$$F(t) = 10 \cdot 10^3 sin(23t). \quad (4.1)$$

This gives a normalized amplitude load function according to Figure (4.7).

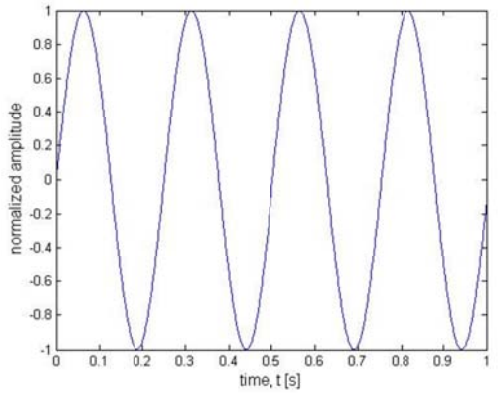

Figure (4.7) *Single frequency harmonic normalized amplitude.*

4.2.5 Impulse load

To investigate the efficiency of the quiet boundaries a simple model consisting of a single continuum part surrounded by semi-infinite elements was established. This model has been loaded with an impulse formed as a half sine wave, Figure (4.8). The used maximum amplitude is 10kN.

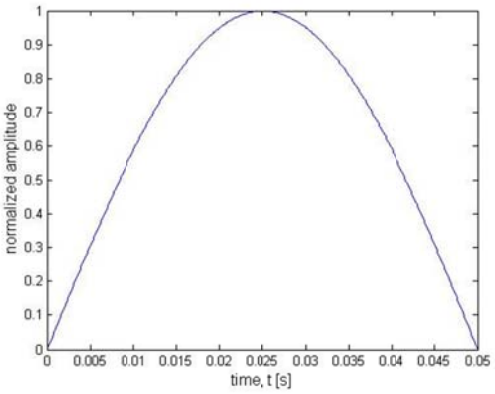

Figure (4.8) *Normalized amplitude of impulse.*

4.3 Solution methods

The standard way of bridge dynamic analysis among Swedish bridge engineers is the use of modal superposition. This requires that the eigenvalue problem is solved and works well in Brigade if the soil-structure interaction is not considered. Instead, direct implicit time integration is applied.

BRIGADE/ABAQUS provides the Hilber-Hughes-Taylor operator for direct time integration. This operation is implicit, meaning that the integration operator matrix must be inverted for every time-step. Solving this set of non-linear equations is highly time expensive. The method is though unconditionally stable, giving that only accuracy in the result increase as the increment decreases [4]. A fixed time-step is used throughout this thesis.

5 CONVERGENCE STUDY

In this chapter a convergence study of the model and the efficiency of the quiet boundaries are studied.

5.1 Convergence

To have a reliable model a convergence test was conducted with respect to both mesh size and time increment. A stationary harmonic load located at the quarter distance of the span, on the rail was applied. Response was recorded in the slab at the same point. No transition increased stiffness was used. Load and response positions are shown in Figure (5.1). The element size convergence test was preformed with a 0.005s time increment and the results are shown in Table (5.1).

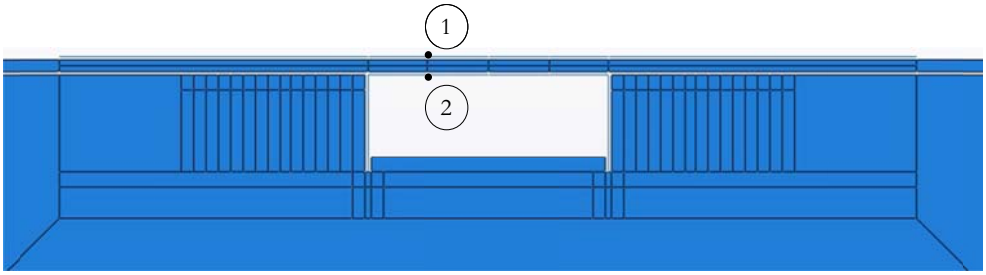

Figure (5.1) *Load and response position. 1. Load position. 2. Response position.*

Table (5.1) *Element convergency.*

Δt	l_e	DOF	f_C	f_{det}	f_{eq}	a_{max}	$diff$
0,005	0,05	358 066	200	80	71 613 200	0,625	-
0,005	0,1	103 728	200	80	20 745 600	0,631	0,88
0,005	0,2	27 620	200	80	5 524 000	0,643	2,80
0,005	0,4	7 965	200	80	1 593 000	0,672	7,52
0,005	0,8	2 572	200	80	514 400	0,724	15,85

Δt	time increment	[s]
l_e	average element size	[m]
DOF	degrees of freedom, number of equations to solve in each increment.	[-]
f_C	calculation frequency, number of increments per second.	[Hz]
f_{det}	approximate maximum detectable frequency if results are picked in each increment (~40% of f_C).	[Hz]
f_{eq}	equation frequency, number of equations needed to be solved for 1s result.	[Hz]
a_{max}	maximum acceleration in steady state.	[m/s²]
$diff$	procentual difference to lowest calculated steady state acceleration.	[%]

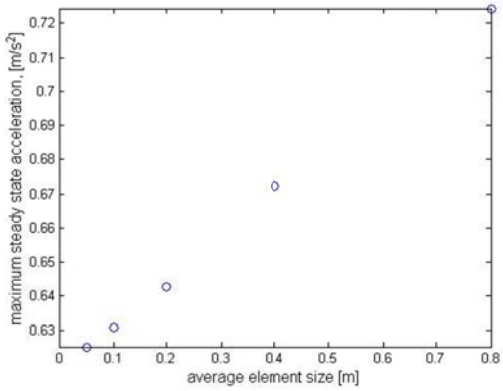

Figure (5.2) *Element convergence results.*

Time increment convergence test was preformed analogous, with an average element size of 0.2m.

Table (5.2) *Increment convergence.*

Δt	l_e	DOF	f_C	f_{det}	f_{eq}	a_{max}	$diff$
0,003	0,2	27 620	400	160	11 048 000	0,64	0,00
0,005	0,2	27 620	200	80	5 524 000	0,643	0,42
0,01	0,2	27 620	100	40	2 762 000	0,656	2,53
0,02	0,2	27 620	50	20	1 381 000	0,71	10,86
0,1	0,2	27 620	10	4	276 200	0,793	23,97

Parameter explanations are given under Table (5.1).

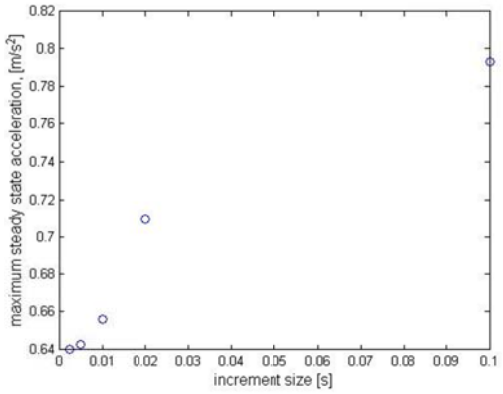

Figure (5.3) *Increment convergence.*

The shear wave speed is far lowest in the soil, making it governing in terms of fitting 8 elements per wavelength. Assuming a frequency of 30 Hz yields (by eq. (2.33)) that the element length can be calculated to

$l_e = \frac{c_s}{8f} = \frac{200m/s}{8x30s^{-1}} = 0.83m.$

Now there are three determining factors for deciding the mesh size.

- Shear wave length term must be fulfilled, reasonable discretization of shortest wavelength.
- Accuracy in response.
- Time step.

For the following analyzes a time increment, Δt, of 0.05s and an element size, l_e of 0.2m is used.

All the acceleration responses of the convergence study are shown as a function of time in

APPENDIX C. It can be noticed that a time increment of 0.1s does not give a satisfactory response.

5.2 Quiet boundaries

There exist two types of energy dissipation in the structure. Materials themselves absorb energy, here assumed as Rayleigh damping. Other than material damping, geometrical damping is of great importance. It concerns the fact that a constant quantity of energy yields strains that spread over an increasing area, giving lower strain magnitudes. To account for this in a finite model, attention has to be paied to the model boundaries. For this study the *ABAQUS* semi-infinite elements CINPS4 are used.

5.2.1 Impulse load exciting continuum

The first study to examine energy dissipation is a continuum excited by an impulse load, this load is described in chapter (4.2.5). Mainly the aim here is to get an indication of the behavior of the quiet boundary. The continuum with one-way infinite elements is shown in Figure (5.4). It is given material parameters as the soil, given by Table (3.5), except from the fact that no Rayleigh material damping is applied.

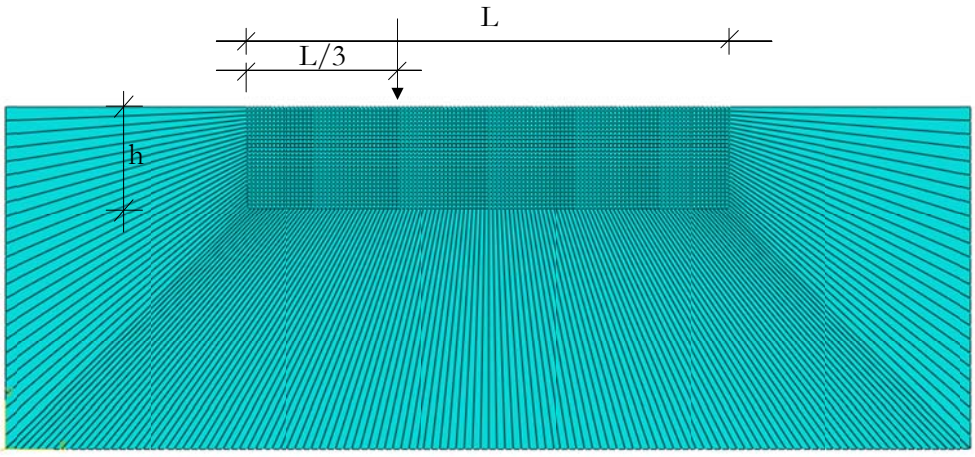

Figure (5.4) *Schematic of loading and mesh, L=180m h=37.5m, element size=1.5m.*

Directly after all the impulse load has been applied the continuum, all of its energy has created strains in the material. These strains give arise to stresses shown in Figure (5.5). Figure (5.6) shows the stresses at the time just before impact with the semi infinite elements. The stresses here are of lower magnitude due to the spread over a larger area, geometrical damping. At the time slightly after impact at the boundary of the semi infinite elements some energy has been reflected back into the continuum. This is visualized in Figure (5.7). After a while when the load has been reflected a few times a somewhat chaos-like pattern is reviled, see Figure (5.8).

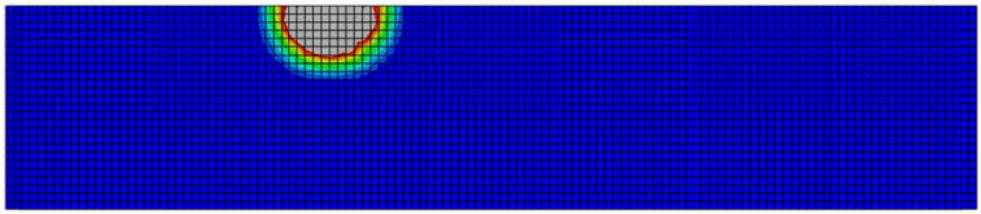

Figure (5.5) *Mises stress at the end frame of the impulse.*

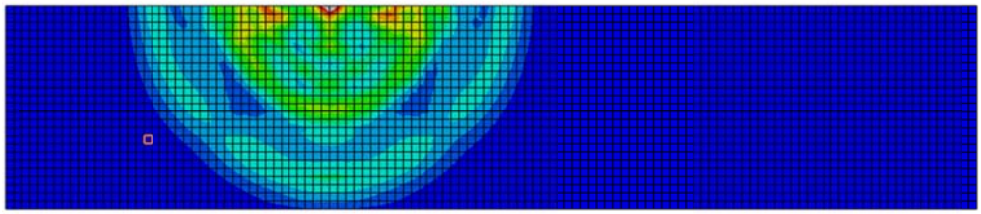

Figure (5.6) *Mises stress at the time just before impact with semi-infinite elements.*

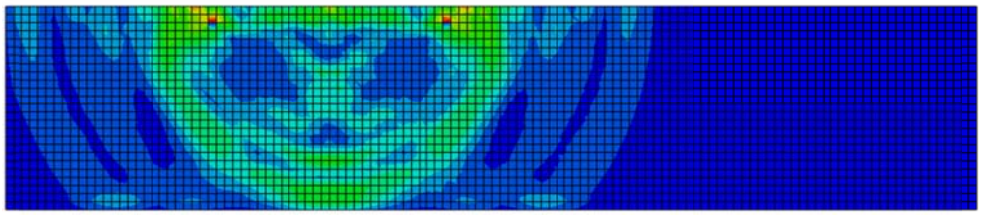

Figure (5.7) *Mises stress at the time slightly after impact with semi-infinite elements.*

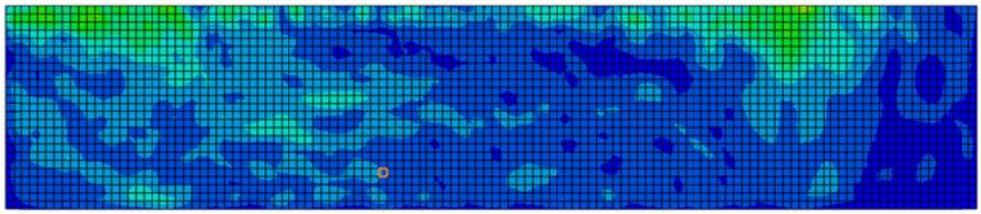

Figure (5.8) *Mises stress a few seconds after impact.*

Energy is shown to be absorbed by the semi-infinite elements but not to a full extent. Thus, the elements provide a quiet but not silent boundary. This is also stated in the *ABAQUS*-manual [4]. In fact only waves that propagate in a 90 degree angle towards the CINPS4-elements are fully absorbed.

5.2.2 Re-creation of transition studies

The study resumed in chapter (2.8) where re-created and results compared. Main difference between the study of chapter (2.8) and the study here lies in the area of energy dissipation. In the previous sub-chapter the boundaries were shown to be silent, but not quiet. How this affects a result will now be investigated. Figure (5.9) shows the schematics of a single continuum model excited by a moving load. An element size of 1.5m for the plain stress elements was used.

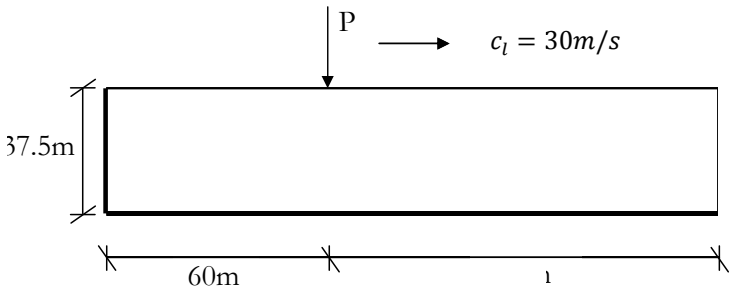

Figure (5.9) *Schematic of continuum model.*

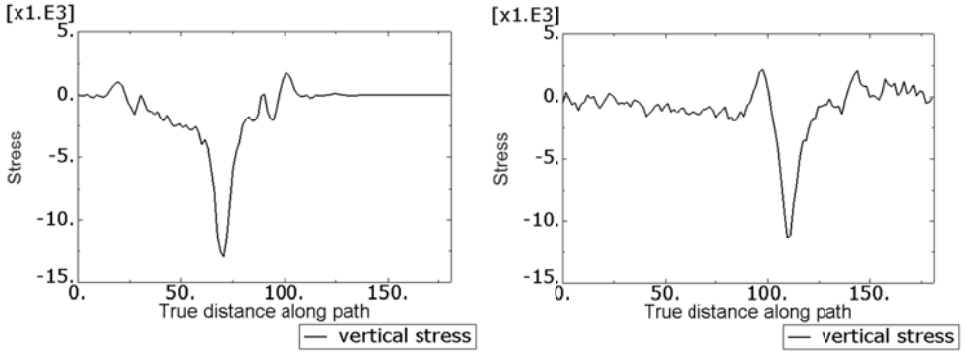

(A) (B)

Figure (5.10) *Vertical stresses after (A) 10m load propagation and (B) 40m load propagation at a distance from the surface of 6m.*

It is here clear that the energy does not completely dissipate as the figures diverge in comparison with Figure (2.14). The reflected energy does not affect the magnitude of the stress peaks (steady state response) in a large sense. Rayleigh waves induced by the sudden load application can be detected in Figure (5.10) (A). Magnitude evaluation of the Rayleigh wave shall though not be performed as the plot shows disturbance, created mainly by energy reflection. In Figure (5.10) no

Rayleigh wave is present due to its high wave-speed, indicating the presence of energy reflection. Comparing the studies the small difference in result position shall be noticed. This is why no exact comparison in absolute values is made.

Another model was created introducing the concept of a stiffness discontinuity in resemblance with the study reviewed in chapter 2.8. Its schematic is visualized in Figure (5.11).

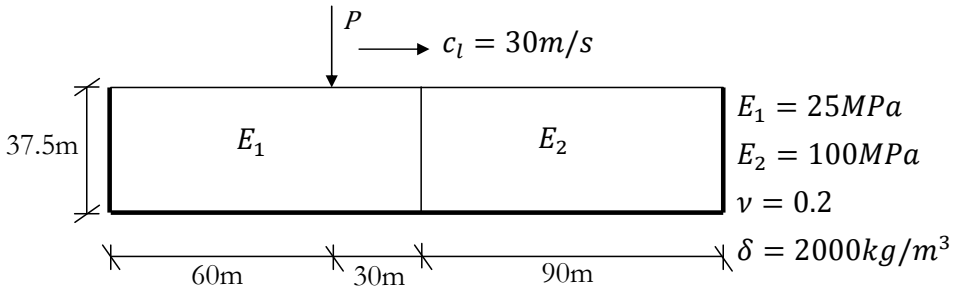

Figure (5.11) *Schematic of model with a stiffness discontinuity.*

Resulting vertical stress at a distance 6m from the surface at different times is shown in Figure (5.12).

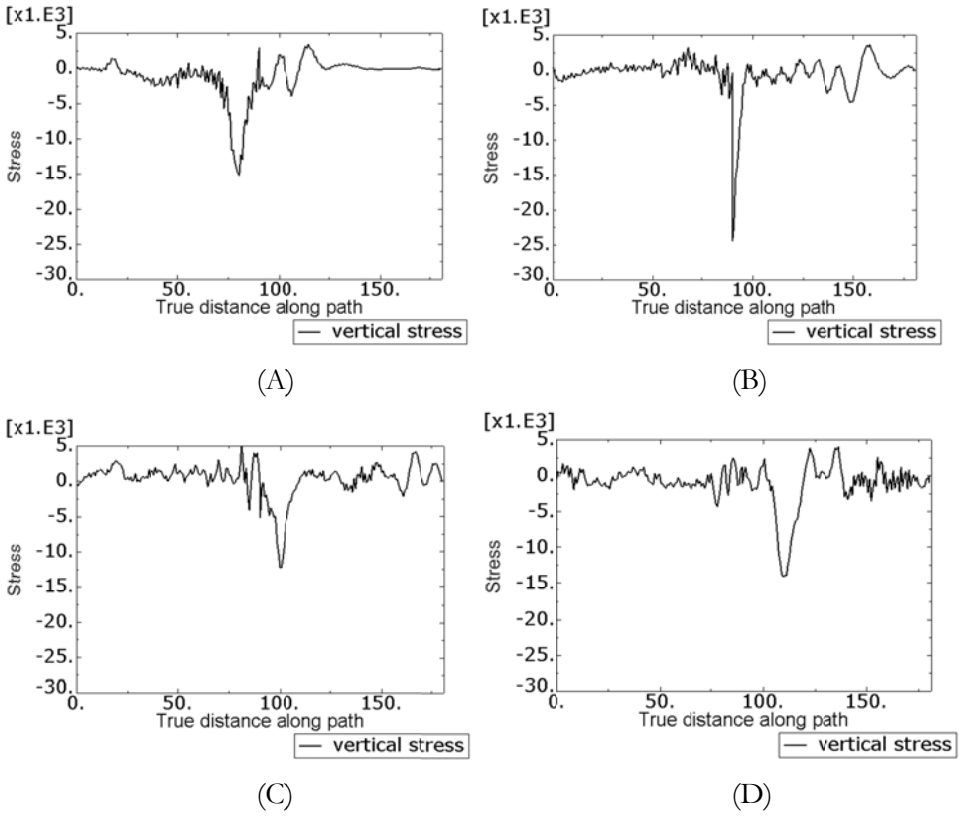

Figure (5.12) *Vertical stress after (A) 20m, (B) 30m, (C) 40m and (D) 50m load propagation.*

Again the steady state response shows good resemblance with chapter 2.8. The low stress peaks from dynamic phenomenon's as reflection and refraction is harder to detect and not appropriate to evaluate in an exact manner due to the boundary reflected energy.

This chapter shows that the modeled structure converges and the use of *ABAQUS* semi infinite elements, CINPS4, give a satisfactory energy absorption.

6 ANALYSIS

6.1 Detection of eigen-frequency

For repeated loading the first eigen-frequency with respect to vertical motions is usually of importance. in this case to detect the first resonance velocity of the train load. To estimate this frequency a frequency sweep is done at a point, L/4 of the span width. This is done instead of a standard eigenvalue extraction procedure since the software used can not handle complex eigenvalues.

The harmonic point load has a magnitude of 10kN. FFT was done using the *MATLAB* function pwelch [11]. See also *MATLAB*-script in APPENDIX G.

Estimated natural frequencies of the main structure will be compared to those of a model with the portal frame structure alone. The structure without soil interaction has pinned boundary conditions.

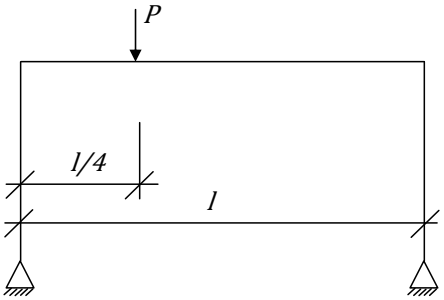

Figure (6.1) *Schematic of the simple frame structure.*

For the case of the model including soil-structure interaction, two frequency sweeps are made. One with no stiffness increase and one with the stiffest transition zone used. This is made as the resonant load velocity is of great importance and a change in lowest resonance frequency due to structural divergence need to be considered.

6.2 Three level design of experiment

To study the influence of the transition zone on the dynamic response of the bridge a structured Design of Experiment (DOE) was employed. Three variables were chosen. A full three level study would induce a large number of calculation runs, instead a three-level Box-Benchen plan [11] was used.

Here the displacement, velocity and acceleration in the quarter point of the span are chosen as representatives of the bridge characteristics. Affecting varied parameters of the study are

- Load velocity, c_l.
- End transition stiffness, E_1.
- Transition zone length, L.

Load velocity is chosen to be on the interval 290-330km/h. The stiffness transition is chosen to have a maximum end stiffness of 10-30GPa. The stiffness is assumed to vary linearly. Each slice has length of 0.2m, Figure (3.5). Transition stiffness length is chosen to vary between 2.8 and 5.2m. The stiffness transition zone is shown in Figure (6.2).

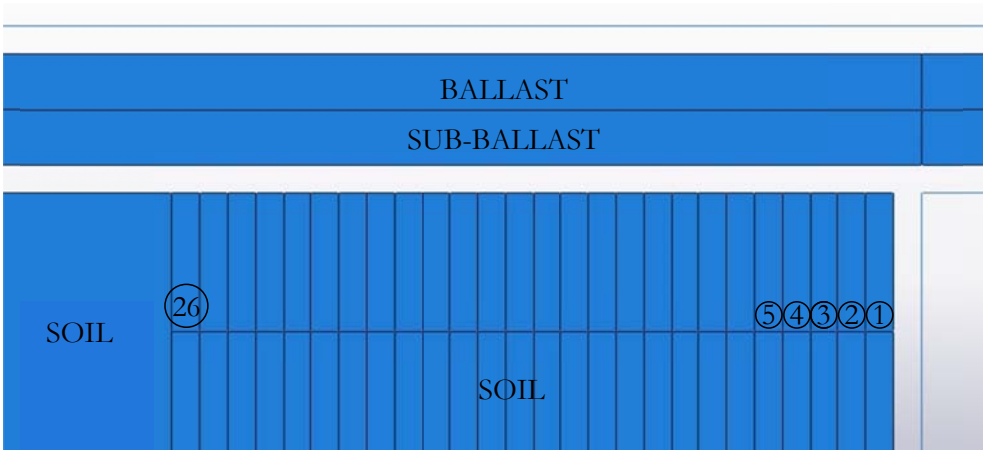

Figure (6.2) *Transition zone composition.*

The design matrix is built using three levels of each parameter. -1 represents low level, 1 high level and 0 a medium level, and is shown in Table (6.1). Numerical values of the levels are shown in Table (6.1).

The exact stiffness's of each run for the transition zone is shown in APPENDIX D.

Table (6.1) *Three level Box-Benchen design matrix.*

Run	c_l	E_1	L
1	-1	-1	0
2	-1	1	0
3	1	-1	0
4	1	1	0
5	-1	0	-1
6	-1	0	1
7	1	0	-1
8	1	0	1
9	0	-1	-1
10	0	-1	1
11	0	1	-1
12	0	1	1
13	0	0	0

Table (6.2) *Numerical values of parameter levels.*

Level	$c_l[km/h]$	E_1 $[GPa]$	L $[m]$
-1	290	10	2.8
0	310	20	4
1	330	30	5.2

Results in terms of displacement, velocity and accelerations at the slab quarter-point are then evaluated using multiple regression analysis in the following manner:

- Full quadratic regression analysis including linear, quadratic and interacting terms.
- Excluding all terms with a significance lower than 80%.
- Modified regression analysis using remaining terms.
- Verifying the statistical analysis with degree of explanation, residual spread and significance.

The full regression analysis yields an estimated regression expression on the form

$$u(c_l, E, L) = \beta_0 + \beta_1 c_l + \beta_2 E_1 + \beta_3 L + \beta_4 c_l E_1 + \beta_5 c_l L + \beta_6 E_1 L + \beta_7 {c_l}^2 + \beta_8 {E_1}^2 + \beta_9 L^2. \quad (6.1)$$

The multiple regression analysis is based on the assumption of normal distribution of residuals. Therefore the residual spread should be constant over the interval of interest. This must be proved to validate a regression run.

The regression analysis was done using the function 'regstats' of the statistics toolbox in *MATLAB*. A separate program was written to read output from *BRIGADE*, carry out the regression analysis and create plots. The program can be found in APPENDIX E.

6.3 Transition length study

In order to study the transition length more in detail, a separate study using a fixed velocity and a fix end stiffness, only varying the length of the transition zone was done. The transition zone length was varied from 0 to 12m in steps of 0.8m. This was made using a linear variation from the soil stiffness to an end stiffness of 30GPa. 16 Runs were made, one without a stiffness transition and 15 runs with

increasing stiffness transition length. The transition zone is displayed in Figure (6.3) where the number of used slices increase from 0 to 15.

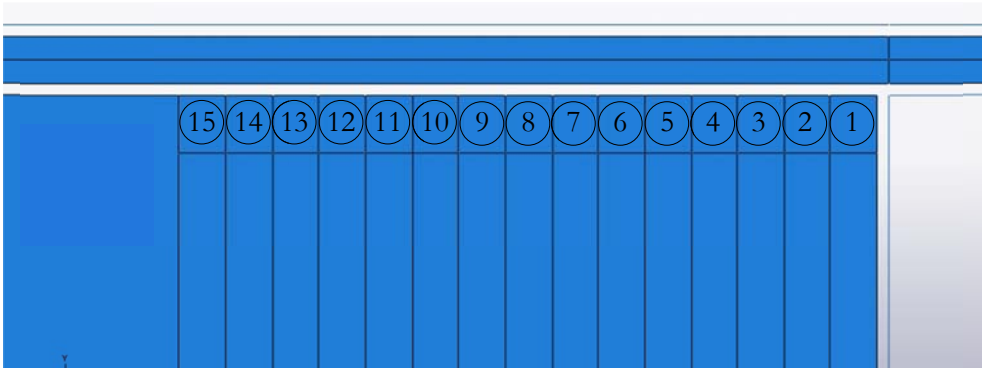

Figure (6.3) *Transition zone of length study.*

Peak displacements from each run was compared to maximum static displacement. and the dynamic amplification factor (DAF) defined as

$$DAF = \frac{u_{max,dynamic}}{u_{max,static}}, \tag{6.2}$$

was calculated. Maximum static deflection of the slab quarter-point is given when the train-load has its center of a twin axis at the bridge centre point. Young's modulus variation of the transition zone for each run is found in APPENDIX 0.

7 RESULTS AND DISCUSSION

7.1 Natural modes and frequencies

In order to investigate the dynamic behavior of the bridge, three cases are used. Case one – the portal frame alone; case two – the portal frame, track structure and the surrounding soil; and case three – the portal frame, track structure, surrounding soil and the transition zone.

A harmonic frequency sweep was applied at L/4 of the bridge span. Acceleration in the same point was recorded. Figure (7.1) through Figure (7.3) show the acceleration response. It can clearly be seen that a large difference exist between the three cases.

For the portal frame alone the response is dominated by two modes. It can also be seen that the response peaks are relative sharp, meaning that the modal damping is low, i.e. dominated by the material damping of the structure.

For the other two cases the response levels are lower and more peaks are visible. Also, all peaks are not sharp, indicating that the modal damping is not dominated by the portal frame alone. The first resonance appears to be lower than for the portal frame alone. Considering the fact that the surrounding soil is included – effects of soil-structure-interaction can be suspected to have changed the dynamic behavior of the portal frame.

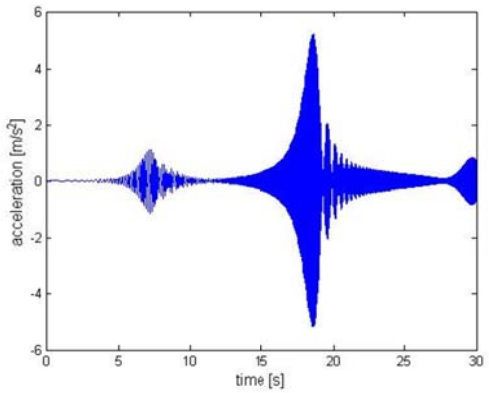

Figure (7.1) *Acceleration time history, portral frame alone.*

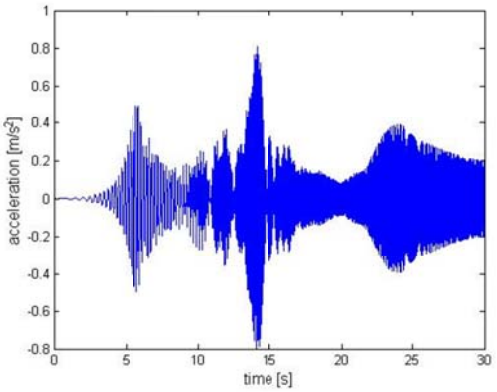

Figure (7.2) *Acceleration time history, full model and no transition stiffness.*

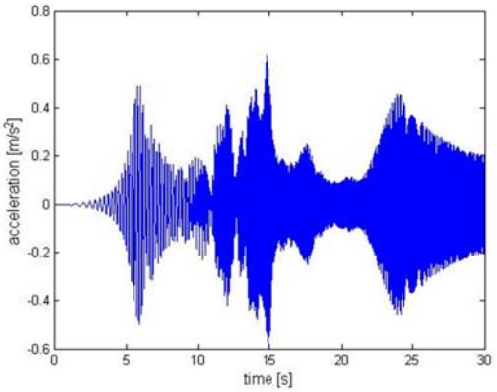

Figure (7.3) *Acceleration time history, full model and stiffest transition zone.*

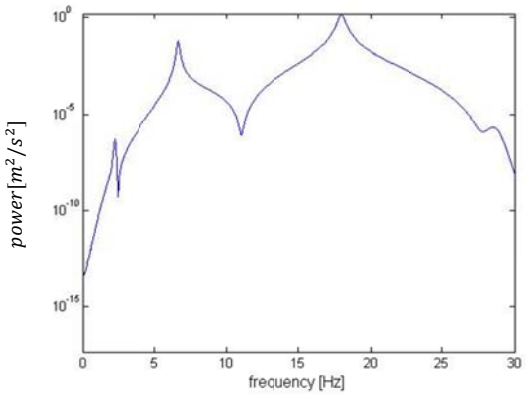

Figure (7.4) *Acceleration PSD at L/4, portal frame alone.*

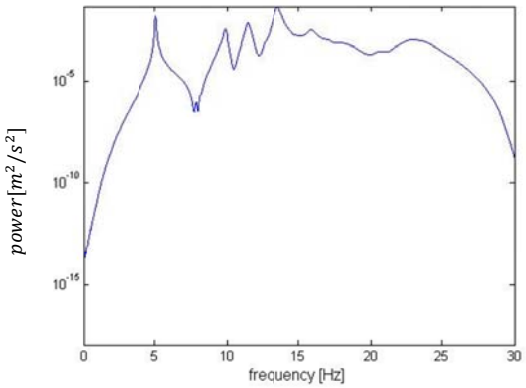

Figure (7.5) *Acceleration PSD at L/4, full model and no transition stiffness.*

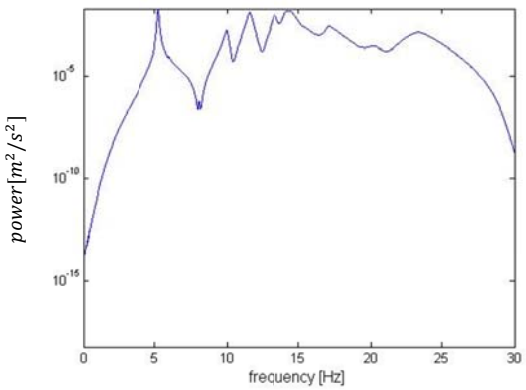

Figure (7.6) *Acceleration PSD at L/4, full model and stiffest transition zone.*

Soil-structure interaction decreases the first natural frequency with respect to vertical deflections by approximately 2Hz in this case.

Comparing Figure (7.5) and Figure (7.6) one can see that the increase of stiffness within the transition zone affects the structure irrelevantly with respect to the first natural frequency.

The first natural frequency of the full model is estimated to 5.1 Hz. Using the distance between two axles in the load model, see Table (4.2), a critical speed of

$$v_{cr} = f_1 D = 5.1\frac{1}{s} \cdot 18m = 91.8\frac{m}{s} \sim 330\frac{km}{h},$$

can be calculated.

7.2 Three level parametric study

The parametric study preformed is described in section 6.2. Maximum results of each resulting parameter are showed in Figure (7.7).

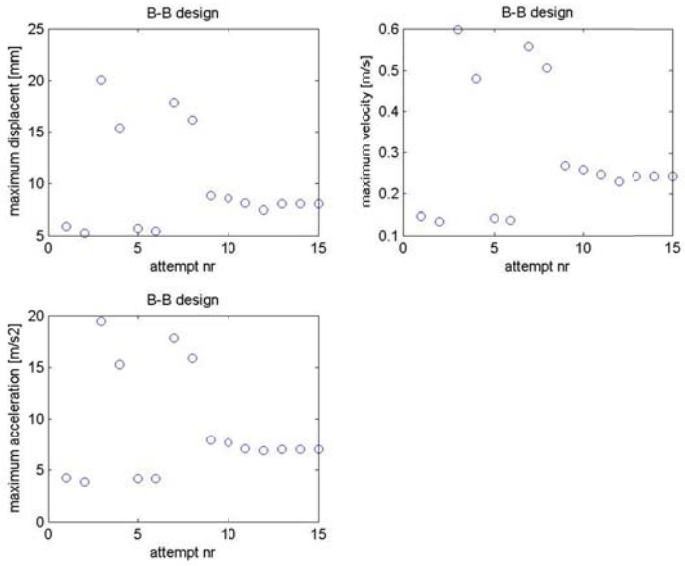

Figure (7.7) *Peak values of each run.*

One may notice that the pattern of the plots are very similar. This suggests that each resulting parameter responds in the same principal manner to a transition stiffness change.

Based on the simulation results a full regression analysis is carried out. The resulting significance are shown in Table (7.1). Green marked fields correspond to coefficients that can be shown to be divergent from zero with significance greater than 80%. Figure (7.8) shows the residuals in a normal probability plot. A good normal spread is shown.

Plotting normalized residuals versus fitted value gives an indication if the normal spread is constant over the interval. This is shown in Figure (7.9).

Table (7.1) *Regression coefficients and corresponding significance levels.*

	a	P_a [%]	v	P_v [%]	u	P_u [%]
β_0	670,68	98,93	17,5246	99,11	0,6706	98,45
β_1	-4,753	99,26	-0,1257	99,4	-0,0048	98,9
β_2	1,2935	88,22	0,0371	91,58	0,0014	87,28
β_3	5,4507	61,91	0,1448	65,23	0,0049	51,94
β_4	-0,0048	92,57	-0,0001	94,29	0	91,47
β_5	-0,0199	72,79	-0,0005	73,07	0	54,51
β_6	0,0003	0,82	-0,0001	14,03	0	15,92
β_7	0,0085	99,45	0,0002	99,57	0	99,16
β_8	0,0027	40,02	0	28,87	0	35,82
β_9	0,0554	12,4	0,0002	1,77	-0,0001	13,41

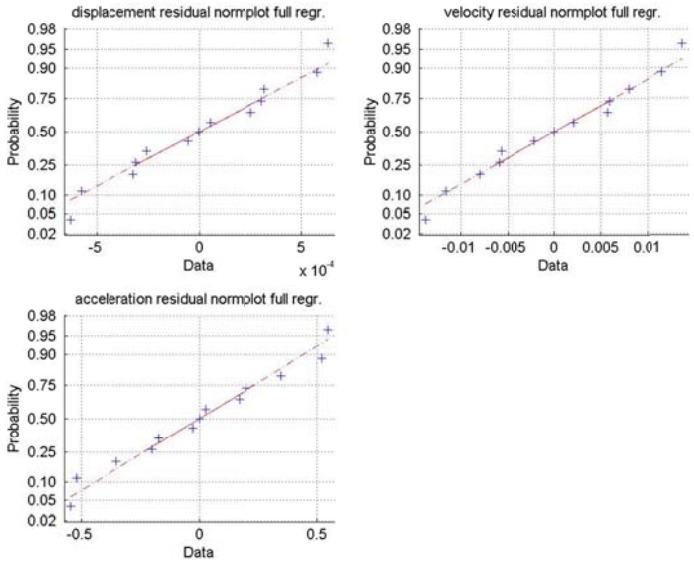

Figure (7.8) *Normal probability plot of residuals; full analysis.*

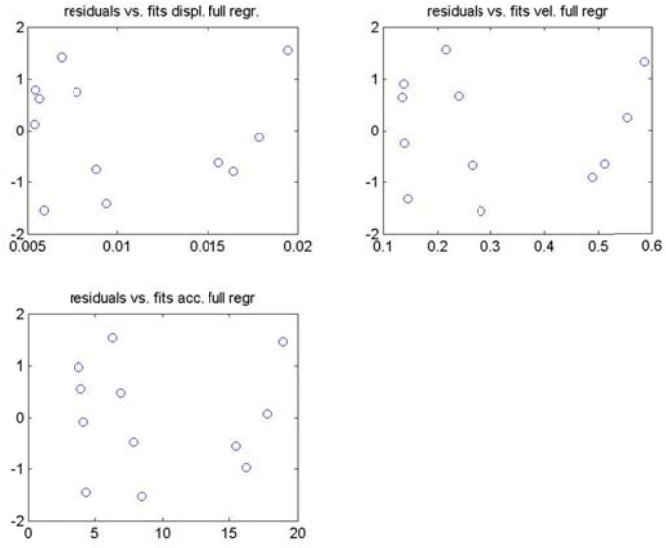

Figure (7.9) *Residual (ordinate) versus fitted value (abscissa), full regression.*

Three groups are clearly shown. These correspond to the different velocity groups as it is the factor of largest impact. The results of the full regression analysis, under the permits given, indicate that the coefficients $\beta_0, \beta_1, \beta_2, \beta_4$ and $, \beta_7$ shall be brought to a modified regression analysis. Resulting in a modified regression function as

$$f(c_l, E, L) = \beta_0 + \beta_1 c_l + \beta_2 E + \beta_4 c_l E + \beta_7 {c_l}^2. \quad (7.1)$$

The degree of explanation for the full regression analysis is over 99% for all the resulting variables.

Coefficients involving the transition zone length can not be guaranteed separated from zero at the 80%-level of significance.

Table (7.2) show the regression coefficients and corresponding significance of the modified regression analysis.

Table (7.2) *Regression coefficients and corresponding significance of the modified regression analysis.*

	a	P_a [%]	v	P_v [%]	u	P_u [%]
β_0	666,99	99,9	17,7341	99,9	0,6753	99,9
β_1	-4,6676	100	-0,125	100	-0,0047	99,9
β_2	1,4048	97,63	0,0384	97,92	0,0015	97,63
β_4	-0,0048	98,13	-0,0001	98,4	0	98,17
β_7	0,0082	100	0,0002	100	0	100

The normal spread of residuals is shown by Figure (7.10).

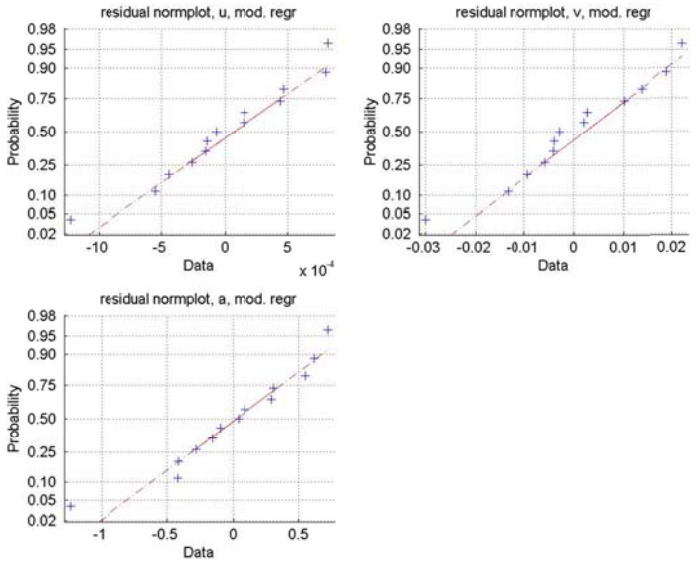

Figure (7.10) *Normal plot of residuals, modified analysis.*

A linear behavior is obtained indicating a reasonable assumption.

The assumption of a constant residual spread over the interval is evaluated by plotting residuals against fitted value, see Figure (7.11).

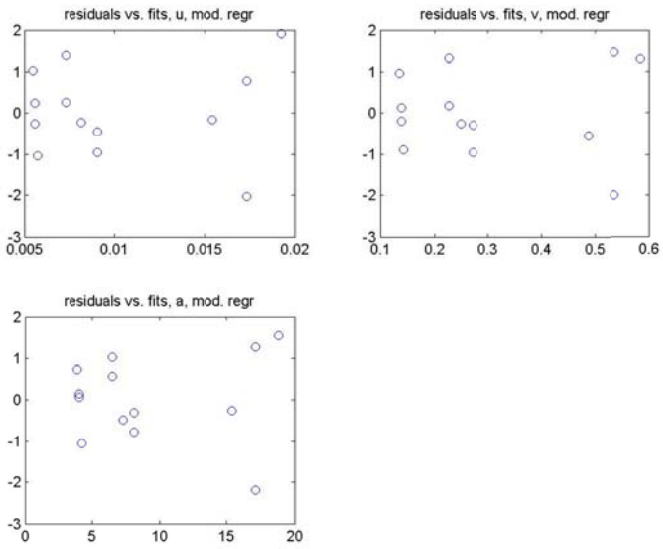

Figure (7.11) *Residuals (ordinate) versus fitted value(abscissa), modified analysis.*

It is observed that the spread of the residuals is somewhat higher at the highest speed, corresponding to the resonant speed. This yields a somewhat higher residual spread than needed. It is though acceptable as a varying residual spread does not affect the principal results [15].

The figures and tables of this section clearly indicate that the speed of the load is a decisive factor for this study. Transition length can not be proved to impact the dynamic behavior of the bridge in the interval 2,8-5,2m at speeds and stiffness's declared above, using this approach. Transition zone end stiffness is shown to give a small but in the context neglectable impact.

Plots were made visualizing the variation of one parameter when the other withholds their 0-level value. This has been done for all three resulting parameters of interest in Figure (7.12) to Figure (7.14).

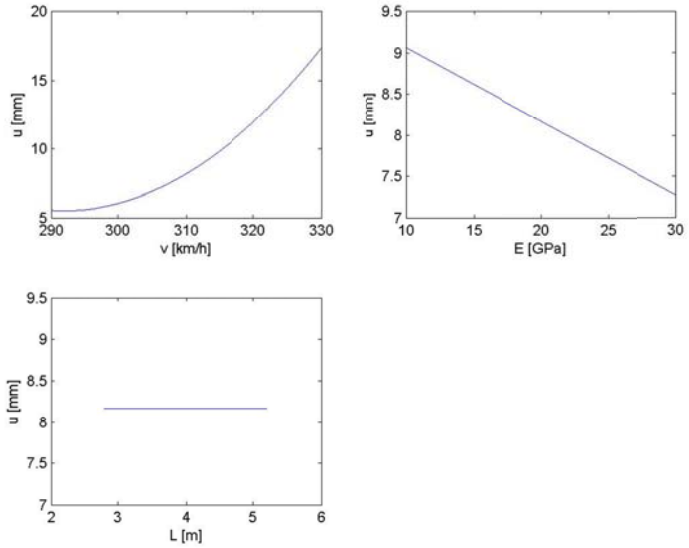

Figure (7.12) *Regression function with respect to displacements of each variation parameter on valid interval (when one parameter is varying the other two withhold their mid value).*

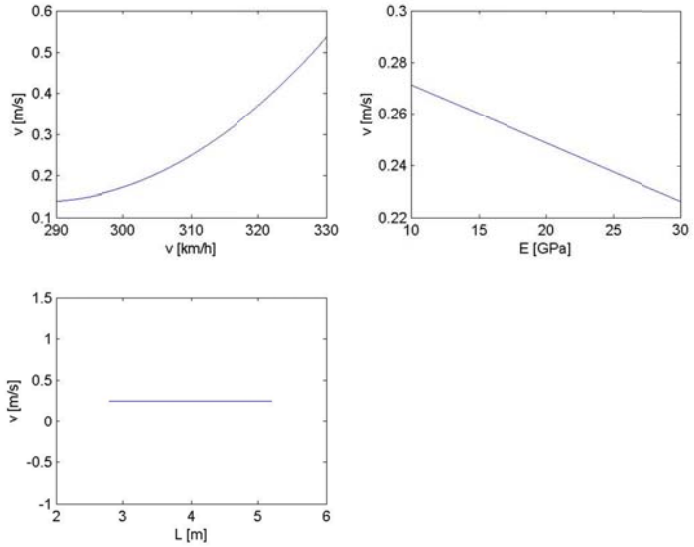

Figure (7.13) *Regression function with respect to velocity of each variation parameter on valid interval (when one parameter is varying the other two withhold their mid value).*

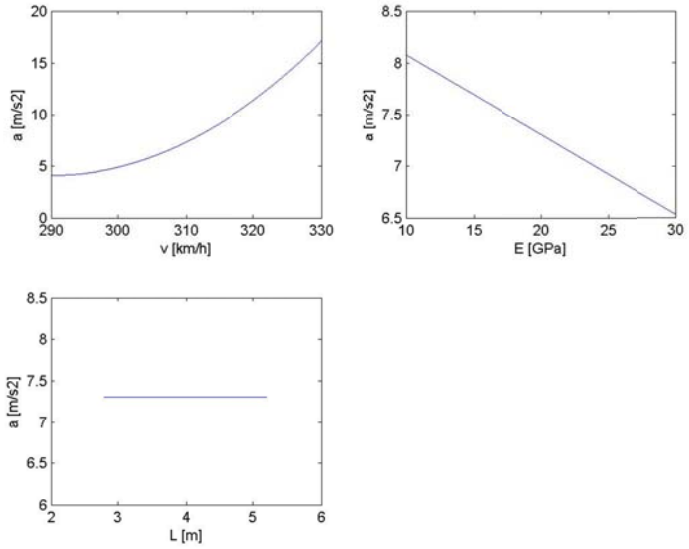

Figure (7.14) *Regression function with respect to acceleration of each variation parameter on valid interval (when one parameter is varying the other two withhold their mid value).*

7.3 Transition length study

In this section the Dynamic Amplification Factor (DAF), with specific focus on displacements is the main target. Three train velocities; 200 km/h, 300 km/h and 400 km/h are chosen. They represent ratios of load velocity by critical velocity, v/v_{cr}, of 0.6, 0.91 and 1.21. v_{cr} is calculated in chapter 7.1. Peak displacement of each run is shown in Table (7.3) where the dead load is subtracted.

The DAF is calculated directly out of Table (7.3) and plotted in Figure (7.15).

Table (7.3) *Deflections of train load.*

Run	$u_{max,\ static}$	$u_{max,\ 200\ km/h}$	$u_{max,\ 300\ km/h}$	$u_{max,\ 400\ km/h}$
0	1,7805	3,4861	8,0152	5,5395
1	1,7329	3,3552	7,2366	5,6950
2	1,7097	3,3445	6,8096	5,7405
3	1,6893	3,2646	6,3701	5,3745
4	1,6758	3,194	6,0525	5,7323
5	1,6675	3,1608	5,9056	5,7111
6	1,6626	3,1487	5,8088	5,6796
7	1,6597	3,1376	5,7534	5,6426
8	1,6578	3,1314	5,7359	5,6072
9	1,6564	3,1175	5,7408	5,5772
10	1,6556	3,1099	5,7395	5,5598
11	1,6549	3,1117	5,7264	5,5557
12	1,6543	3,1077	5,7246	5,5536
13	1,6539	3,0998	5,7249	5,5459
14	1,6534	3,0985	5,7206	5,5394
15	1,6530	3,0958	5,7172	5,5494

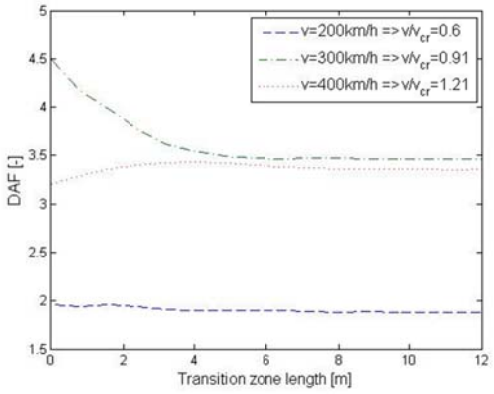

Figure (7.15) *Dynamic amplification factor (DAF) as a function of transition zone length.*

Figure (7.15) clearly indicates that the transition stiffness gives the largest impact around the resonance velocity. It also indicates a point where increasing the transition length give no further positive contribution to the structure. In this case a transition zone length of 4m appears to sufficient. Comparing the DAF with those from the case of two solid materials reveal differences and similarities. Similarly the increasing effect due to speeds close to a resonant speed is shown.

The magnitude of the stiffness transition impact is lower in the case of a full modeled bridge with soil-structure interaction.

8 CONCLUDARY REMARKS AND FURTHER DEVELOPMENTS

The result from this work show that including surrounding soil and a transition zone in the analysis of a portal frame bridge influence the bridge behavior.

It was also found that a limiting length of the transition zone existed in terms of reducing bridge response.

The load used was a moving point load, but in a more realistic case the wheel-rail interaction and further the vehicle dynamics may need to be included. In addition, settlement between surrounding soil and the bridge and track irregularities could be motivated to be considered.

Using a non-linear contact condition between the wheel and the train gives a possibility for separation, and simulation of the jump 'n' bump phenomenon.

A full 3D-study would allow more correct representation of the soil – structure – interaction phenomenon, [16].

Other distributions of stiffness variation, besides linear, in the transition zone may influence result.

REFERENCES

[1] Fryba L, (1972), *Vibration of solids and structures under moving loads,* Thomas Telford Ltd, ISBN: 978-0-7277-3539-3.

[2] Suiker A.S.J., Esveld C., (1997), *Stiffness transition subjected to instantaneous moving load passages*, Delft University of technology.

[3] Inman Daniel J., (2001), *Engineering vibrations*, Pearson Education Inc. ISBN 13: 978-0-13-136311-3.

[4] Dassault Systems, 2007. *Abaqus Analysis 6.7 User's Manual*. Simulia Inc.

[5] Eurocode, (2004), Eurocode 2: *Design of concrete structures,* European committee for Standardization.

[6] Eurocode, (2004), Eurocode 3: *Design of steel structures,* European committee for Standardization.

[7] Möller B.,Larsson B., Bengtsson P-E., Moritz L., (2000), *Geodynamik I praktiken,* Swedish geotechnical institute.

[8] Banverket and Vägverket (2009), *Tekniska kravdokument Geo*, ISSN: 1401-9612.

[9] Jonsson J., (2000), *On ground and structural vibrations related to railway traffic*, Chalmers University of Tehnology, ISBN: 91-7197-920-4.

[10] Eurocode, (2004), Eurocode 1: *Actions on structures,* European committee for Standardization.

[11] The Mathworks Inc. (2008), *MATLAB help files.*

[12] Kramer S., (1996), *Geotechnical earthquake engineering*, Prentice-Hall civil engineering, ISBN: 0-13-374943-6

[13] Ewins D.J., (1984) *Modal Testing: Theory and practice*, John Wily & sons inc., ISBN: 0-471-990472-4.

[14] Banverket (2006), *Måttuppgifter för räler och tungämnen*, BVH 524.12

[15] Vännman, K.., (2009), *Regressionsanalys,* Luleå University of Technology.

[16] Wolf, J.P., Meek, J.W., (1994), *Insight on 2D- versus 3D-moddelling of surface foundations via strength-of-materials solutions for soil dynamics*, John Wily & sons, Ltd.

A APPENDIX A
IMPULSE DERIVATION OF RESPONSE SPECTRA

An impulse load is described by two phases, phase I during the load and phase II after loading as a free vibration with initial conditions from the end of phase I. For lightly damped systems the damping is not valid until a few cycles of vibration. This makes damping negligible for short duration loads and only the undamped case will be considered here.

To compare the different impulse loads a dynamic amplification factor (DAF) will be used defined by the dynamic/static deflection ratio

$$D = \frac{x_{max}}{x_{st}} = x_{max}\frac{k}{P_0}. \quad \text{(A.1)}$$

The results will be published in a response spectra showing the DAF as a function of the load duration.

Triangular suddenly applied impulse load

The triangular suddenly applied impulse load is shown in Figure (A.1).

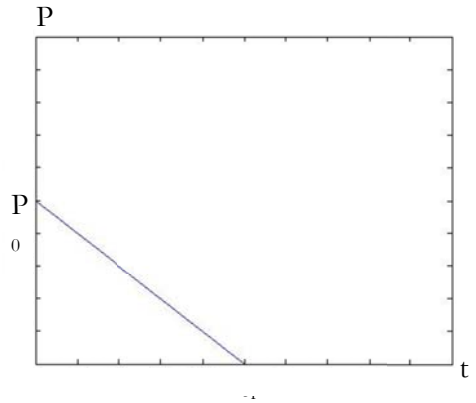

Figure (A.1) *Triangular suddenly applied load.*

Here will follow a derivation of the DAF for the undamped SDOF system subjected to a triangular suddenly applied load. It will be shown in the two phases described above.

PHASE I

The equation of motion, can be written on the form

$$\ddot{x} + \omega^2 x = P(t)/m, \tag{A.2}$$

where

$$P(t) = P_0 - \frac{P_0}{t_1} t, \quad t \in [0, t_1]. \tag{A.3}$$

Approach for particular solution:

$$x_p = a_1 + a_2 t \tag{A.4}$$

Inserting (A.4) in (A.2) yields

$$\omega^2 a_1 + \omega^2 a_2 t = \frac{P_0}{m} - \frac{P_0}{t_1 m} t. \tag{A.5}$$

The constant and linear term has to be equal on each side, yielding

$$a_1 = \frac{P_0}{\omega^2 m} = \frac{P_0}{k} = x_{st} \tag{A.6}$$

$$a_2 = -\frac{P_0}{\omega^2 m t_1} = -\frac{x_{st}}{t_1}. \tag{A.7}$$

Inserting the constants in (A.4) gives the particular solution

$$x_p = x_{st}(1 - \frac{t}{t_1}). \tag{A.8}$$

The general solution is

$$x(t) = A_1 \cos(\omega t) + A_2 \sin(\omega t) + x_{st}(1 - \frac{t}{t_1}), \tag{A.9}$$

with the derivative

$$\dot{x} = -A_1 \omega \sin(\omega t) + A_2 \omega \cos(\omega t) - \frac{x_{st}}{t_1}. \tag{A.10}$$

A_1 and A_2 are constants of integration solved by the initial conditions $x(0) = \dot{x}(0) = 0$, this gives

$$A_1 = -x_{st} \tag{A.11}$$

$$A_2 = \frac{x_{st}}{\omega t_1}. \tag{A.12}$$

Introducing the loading ratio X

$$X = \frac{t_1}{T}, \tag{A.13}$$

where T is the period of one oscillation

$$T = \frac{2\pi}{\omega}. \tag{A.14}$$

The constants of integration of eq. (A.11) and (A.12) in the general solution with definitions of (A.13) and (A.14) yields

$$x(t) = x_{st}\left(\frac{1}{2\pi X}sin(\omega t) - cos(\omega t) + 1 - \frac{t}{t_1}\right). \quad \text{(A.15)}$$

Determining the maximum displacement during the loading phase

This is done by finding the position of zero derivative.

$$\frac{dx}{dt} = 0 \Leftrightarrow$$

$$cos(\omega t) + 2\pi X sin(\omega t) = 1. \quad \text{(A.16)}$$

Using a re-writing technique towards a single sinus term with a phase shift gives

$$\sqrt{1 + 4(\pi X)^2}\, sin(\omega t + \Phi) = 1. \quad \text{(A.17)}$$

Where

$$\Phi = arctan\left(\frac{1}{2\pi X}\right). \quad \text{(A.18)}$$

Using the definition

$$R = \frac{1}{\sqrt{1+4(\pi X)^2}} \text{ and} \quad \text{(A.19)}$$

$$S = arcsin(R) \quad \text{(A.20)}$$

gives

$$sin(\omega t + \Phi) = R. \quad \text{(A.21)}$$

Eq. (A.21) has two solutions

$$S = \omega t + \Phi + n2\pi \text{ , and} \quad \text{(A.22)}$$

$$S = \pi - (\omega t + \Phi) + n2\pi, \quad \text{(A.23)}$$

which gives the time solutions

$$t = \frac{1}{\omega}\{S - \Phi - n2\pi\} = \frac{1}{\omega}t_{n1} < t_1, \text{ and} \quad \text{(A.24)}$$

$$t = \frac{1}{\omega}\{\pi(2n+1) - S - \Phi\} = \frac{1}{\omega}t_{n2} < t_1 \quad \text{(A.25)}$$

To ensure that $t < t_1$ the following restrictions are made for the integer n of each solution

$$n > \frac{1}{2\pi}[S - \Phi - 2\pi X)], \text{and} \qquad n \in \mathbb{N} \quad \text{(A.26)}$$

$$n < \frac{1}{2\pi}[\pi(2X - 1) + s + \Phi]. \qquad n \in \mathbb{N} \quad \text{(A.27)}$$

It also has to be ensured that t>0 by the integer n. This is equivalent with t_{n1}>0, which yields

$$n < \frac{1}{2\pi}(S - \Phi) \quad \text{(A.28)}$$

$$n > \frac{1}{2\pi}(S + \Phi - \pi). \quad \text{(A.29)}$$

Inserting the times of zero derivative (A.24) and (A.25) into (A.15) and using the definition of the dynamic amplification factor in gives

$$D_{phase\ I} = \frac{1}{2\pi X}\{sin(t_{ni}) - t_{ni}\} - cos(t_{ni}) + 1\ i \in 1{,}2 \tag{A.30}$$

PHASE II

To determine the motions in phase II a free undamped vibrations is solved. The constants of integration in can be solved with initial conditions giving

$$x(t) = \frac{\dot{x_0}}{\omega} sin\omega t + x_0 cos\omega t\ , \tag{A.31}$$

where the initial conditions used are from the end of phase I at $t = t_1$ in eq. (A.15).

$$x_0 = x_{phI}(t = t_1) = x_{st}\left\{\frac{1}{2\pi X} sin(2\pi X) - cos(2\pi X)\right\} = x_{st}C_2 \tag{A.32}$$

$$\dot{x_0} = \dot{x_{phI}}(t = t_1) = x_{st}\omega\left\{\frac{1}{2\pi X} cos(2\pi X) + sin(2\pi X) - \frac{1}{2\pi X}\right\} = x_{st}C_1. \tag{A.33}$$

Eq. (A.32) and (A.33) inserted in eq. (A.31) yields

$$x(t) = x_{st}\{C_1 sin\omega t + C_2 cos\omega t\}. \tag{A.34}$$

This oscillation reaches its maximum at

$$\omega t = arctan\left(\frac{C_1}{C_2}\right). \tag{A.35}$$

Eq. (A.35) and use of the DAF definition gives

$$D_{phase\ II} = C_1 sin\left\{arctan\left(\frac{C_1}{C_2}\right)\right\} + C_2 cos\left\{arctan\left(\frac{C_1}{C_2}\right)\right\}. \tag{A.36}$$

Now the dynamic amplification factors are computed as pure functions of the load duration ratio X and one can draw a response spectra by choosing the maximum DAF for each X. The maximum DAF can appear in either in phase I or II. If the load is short it may not exist a local maximum in phase I given by the restrictions of n.

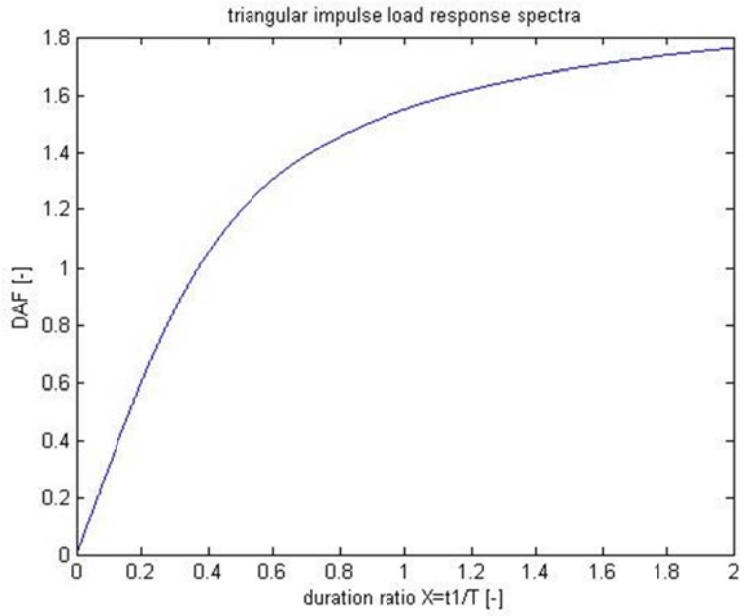

Figure (A.2) *Response spectra for a suddenly applied triangular load.*

Rectangular impulse

The rectangular load is shown in Figure (A.3).

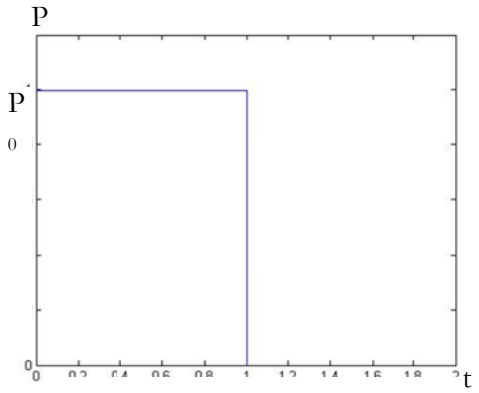

Figure (A.3) *Rectangular load as a function of time.*

PHASE I

The equation of motion, can be written on the form

$$\ddot{x} + \omega^2 x = P(t)/m, \tag{A.37}$$

where

$$P(t) = P_0, \quad t \in [0, t_1]. \tag{A.38}$$

Approach for particular solution:

$$x_p = c \tag{A.39}$$

Inserting (A.39) in (A.37) yields

$$c = \frac{P_0}{m\omega^2} = x_{st}. \tag{A.40}$$

This gives the general solution

$$x(t) = A_1\, sin(\omega t) + A_2\, cos(\omega t) + x_{st} \tag{A.41}$$

$$\dot{x}(t) = A_1 \omega\, cos(\omega t) - A_2\, sin(\omega t). \tag{A.42}$$

With the initial conditions $x(0) = \dot{x}(0) = 0$ the constants of integration is

$$A_1 = 0 \tag{A.43}$$

$$A_2 = -x_{st}, \tag{A.44}$$

which gives

$$x(t) = x_{st}\{1 - cos(\omega t)\} \tag{A.45}$$

$$\dot{x}(t) = x_{st}\omega sin(\omega t) \quad \text{(A.46)}$$

Determining the maximum displacement during the loading phase

Using eq. (A.45) to get the zero derivative point yields

$$sin(\omega t) = 0. \quad \text{(A.47)}$$

Eq. (A.47) has two solutions and they will be presented together below.

$$\omega t + n2\pi = arcsin(0) = 0 \quad \text{(A.48)}$$

$$\pi - \omega t + n2\pi = arcsin(0) = 0, \quad \text{(A.49)}$$

which gives the times of the extreme values

$$t = \frac{1}{\omega}\{n2\pi\} = \frac{1}{\omega}t_{n1} \quad \text{(A.50)}$$

$$t = \frac{1}{\omega}\{\pi + n2\pi\} = \frac{1}{\omega}t_{n2}. \quad \text{(A.51)}$$

To ensure positive t the following restrictions of n is made

$$n > 0 \quad \text{(A.52)}$$

$$n > -0.5. \quad \text{(A.53)}$$

In phase I $t < t_1$which gives

$$t_{n1} < t_1 \Leftrightarrow n < X \quad \text{(A.54)}$$

$$t_{n2} < t_1 \Leftrightarrow n < X - 0.5. \quad \text{(A.55)}$$

Inserting (A.50) and (A.51) in (A.46) with above restrictions in n gives the DAF of phase 1

$$D_{phase\ I} = x_{st}\{1 - cos(t_{ni})\}. \quad \text{(A.56)}$$

PHASE II

To determine the motions in phase II again a free undamped vibration is solved. The constants of integration in can be solved with initial conditions giving

$$x(t) = \frac{\dot{x_0}}{\omega}sin\omega t + x_0 cos\omega t\ , \quad \text{(A.57)}$$

where the initial conditions used are from the end of phase I at $t = t_1$ in eq. (A.46)

$$x_0 = x_{phI}(t = t_1) = x_{st}\{1 - cos(2\pi X)\} = x_{st}C_2 \quad \text{(A.58)}$$

$$\dot{x_0} = \dot{x_{phI}}(t = t_1) = x_{st}\omega\, sin(2\pi X) = x_{st}\omega C_1. \quad \text{(A.59)}$$

Eq. (A.58) and (A.59) inserted in eq. (A.57) yields

$$x(t) = x_{st}\{C_1 sin\omega t + C_2 cos\omega t\}. \quad \text{(A.60)}$$

This oscillation reaches its maximum at

$$\omega t = arctan\left(\frac{C_1}{C_2}\right). \tag{A.61}$$

Eq. (A.61) in (A.60) and use of the DAF definition gives

$$D_{phase\ II} = C_1 sin\left\{arctan\left(\frac{C_1}{C_2}\right)\right\} + C_2 cos\left\{arctan\left(\frac{C_1}{C_2}\right)\right\}. \tag{A.62}$$

Determining the largest DAF for each X gives the response spectra of Figure (A.4).

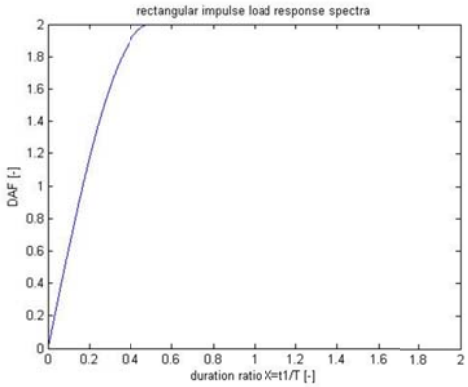

Figure (A.4) *Response spectra for a rectangular impulse.*

Sine-formed impulse

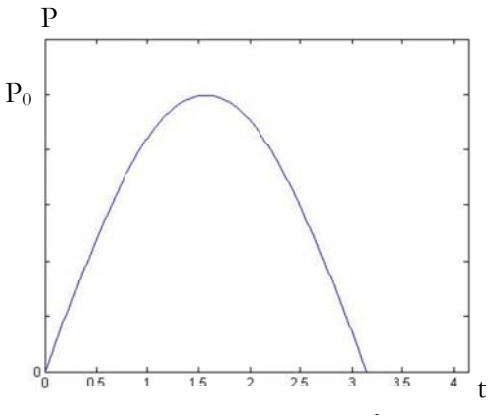

Figure (A.5) *Sine-formed impulse load.*

A sine-formed load,

$$P(t) = P_0 sin(\omega_P t) \quad \text{(A.63)}$$

inserted into the equation of motion, eq. (A.2) , can be shown to have the solution

$$x(t) = x_{st} \frac{1}{1-\beta^2}\{sin(\omega_P t) - \beta sin(\omega t)\}, \quad \text{(A.64)}$$

where:

$\beta = \frac{\omega_P}{\omega}$, loading ratio, [-]. (A.65)

The following relationships and definitions are also valid

$$\hat{\beta} = \frac{1}{1-\beta^2} \quad \text{(A.66)}$$

$$\omega_P = \frac{\pi}{t_1}, \quad \text{(A.67)}$$

$$t_1 = XT = \frac{2\pi X}{\omega}. \quad \text{(A.68)}$$

PHASE I

The derivative of eq. (A.64) with re-writings of eq. (A.65) to (A.68)

$$\dot{x}(t) = x_{st}\hat{\beta}\omega_P\{cos(\omega_P t) - cos(\omega t)\}, \quad \text{(A.69)}$$

has the zero solution

$$\omega_P t = \pm\omega t + n2\pi. \quad \text{(A.70)}$$

Again there exists two separate solutions. The first one,

$$t = \frac{n2\pi}{\omega_P - \omega} = t_1 \frac{2n}{1-2X} = t_1 t_{n1}, \tag{A.71}$$

can be shown to be valid if and only if

$$X > \frac{3}{2}. \tag{A.72}$$

The second solution,

$$t = \frac{n2\pi}{\omega_P + \omega} = t_1 \frac{2n}{1+2X} = t_1 t_{n2}, \tag{A.73}$$

has due to the conditions, $t < t_1$ and $t > 0$, the restrictions

$$n > 0, n < \frac{1}{2} - X. \tag{A.74}$$

Inserting the time solutions and using the DAF definition yields

$$D_{phase\ II}(X) = \hat{\beta}\{sin(t_{ni}) - \beta sin(2\pi X t_{ni})\} \tag{A.75}$$

PHASE II

$$x(t) = \frac{\dot{x_0}}{\omega} sin\omega t + x_0 cos\omega t\ , \tag{A.76}$$

where the initial conditions used are from the end of phase I at $t = t_1$ in eq. (A.64)

$$x_0 = x_{phI}(t = t_1) = -x_{st}\hat{\beta}\beta sin(2\pi X) = x_{st} C_2 \tag{A.77}$$

$$\dot{x_0} = \dot{x_{phI}}(t = t_1) = -x_{st}\hat{\beta}\omega_P\{1 - sin(2\pi X)\} = x_{st}\hat{\beta}\omega_P C_1. \tag{A.78}$$

Eq. (A.77) and (A.78) inserted in eq. (A.76) yields

$$x(t) = -x_{st}\hat{\beta}\beta\{C_1 sin\omega t + C_2 cos\omega t\}. \tag{A.79}$$

This oscillation reaches its maximum at

$$\omega t = arctan\left(\frac{C_1}{C_2}\right). \tag{A.80}$$

The time solution and use of the DAF definition gives

$$D_{phase\ II} = C_1 sin\left\{arctan\left(\frac{C_1}{C_2}\right)\right\} + C_2 cos\left\{arctan\left(\frac{C_1}{C_2}\right)\right\}. \tag{A.81}$$

Determining the largest DAF for each X gives the response spectra of Figure (A.6).

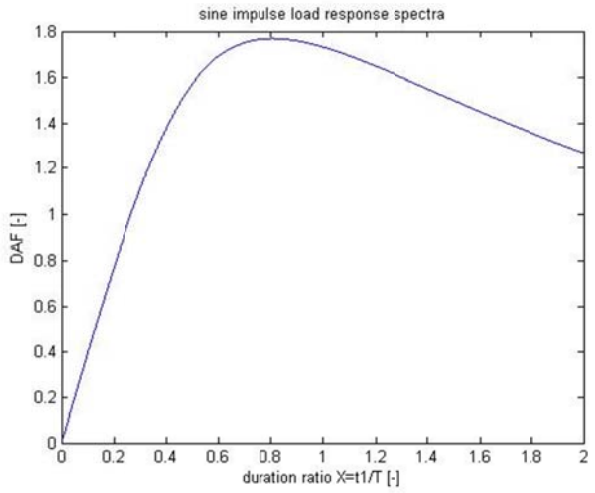

Figure (A.6) *Response spectra for a sine-formed impulse.*

The three different response spectras are collected in Figure (A.7).

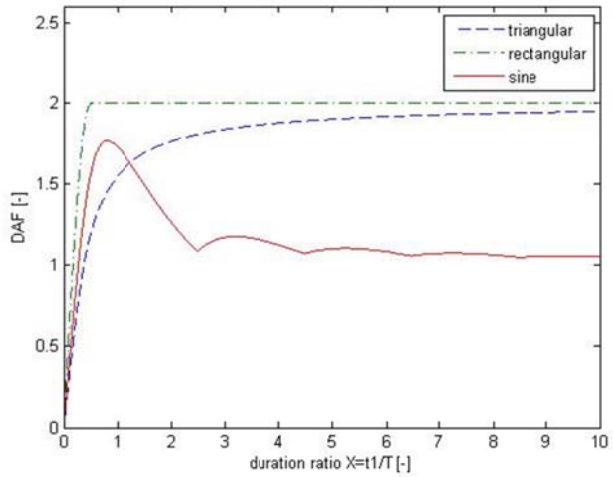

Figure (A.7) *Response spectra for three different impulse forms.*

One can now conclude that if a load is applied suddenly the DAF will converge towards 2. If the load if slow enough the response will be quasi-statiq and the DAF converges towards 1.

B APPENDIX B

SVEP.m

```
%%% Using chirp        %%%
%%% By: Peter Nilsson  %%%

clear all
close all
clc

t=0:0.001:30;
f0=0.1;
f1=30;
t1=max(t);
phi=-90;
F=chirp(t,f0,t1,f1,'linear',phi);
plot(t,F)
xlabel('\fontsize{12}time, t [s]')
ylabel('\fontsize{12}amplitude, A [-]')

F=[t;F];

%%%% Skapar full lastsignal som används i Brigade
fid = fopen('frekvenssvep.txt', 'wt');
fprintf(fid, '%6.6f %16.8f\n', F);
fclose(fid);
%%%%%%%%%%%%%%%%%%%%%%%%%%%%%%%%%%%%%%%%%%%%%%%%%%

%%%% Skapar lastsignal i var tredje tidssteg som används för signalanalys
F_n3=[F(1,1:3:length(F(1,:)));F(2,1:3:length(F(1,:)))];

fid = fopen('force_signal_n_3.txt', 'wt');
fprintf(fid, '%6.6f %16.8f\n', F_n3);
fclose(fid);
```

C APPENDIX C
CONVERGENCE PLOTS

ELEMENT CONVERGENCE

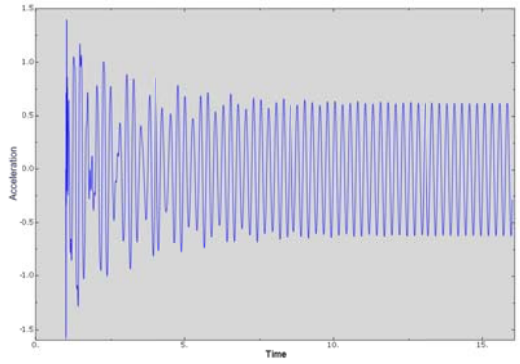

Figure (C.1) *Time increment = 0.05s, element size=0.05m.*

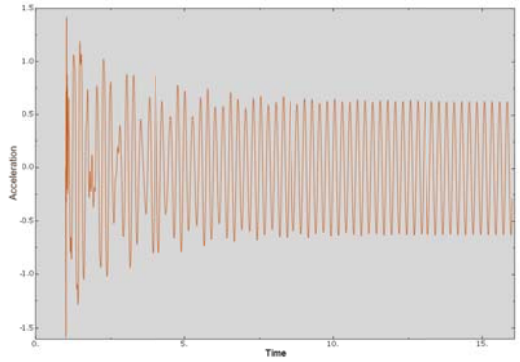

Figure (C.2) *Time increment = 0.05s, element size=0.1m.*

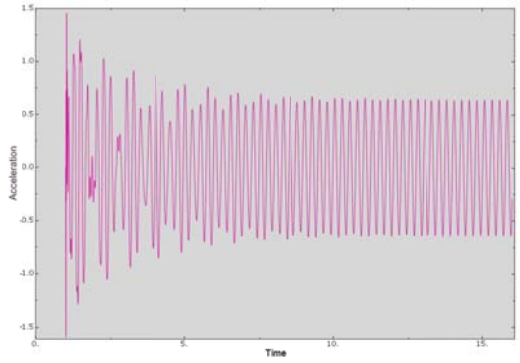

Figure (C.3) *Time increment = 0.05s, element size=0.2m.*

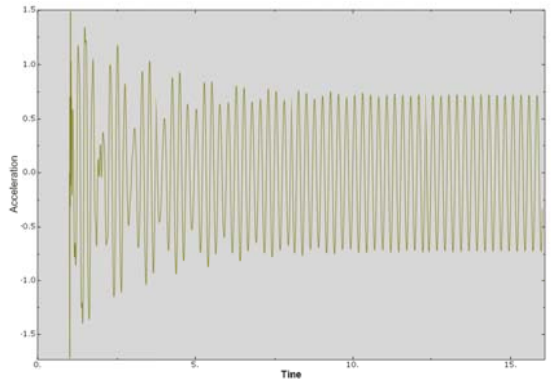

Figure (C.4) *Time increment = 0.05s, element size=0.4m.*

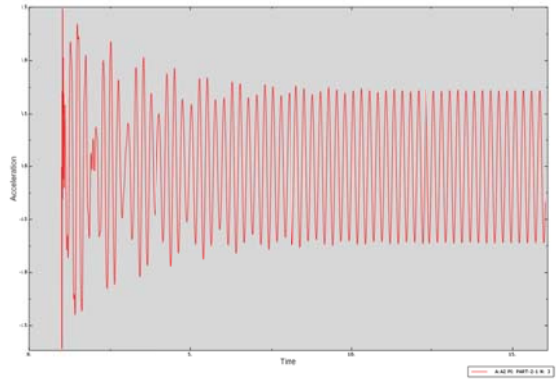

Figure (C.5) *Time increment = 0.05s, element size=0.8m.*

INCREMENT CONVERGENCE

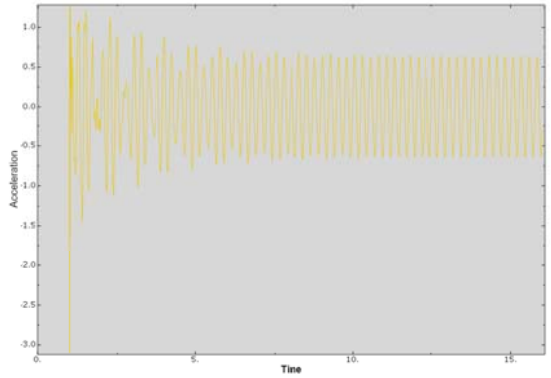

Figure (C.6) *Time increment = 0.0025s, element size=0.2m.*

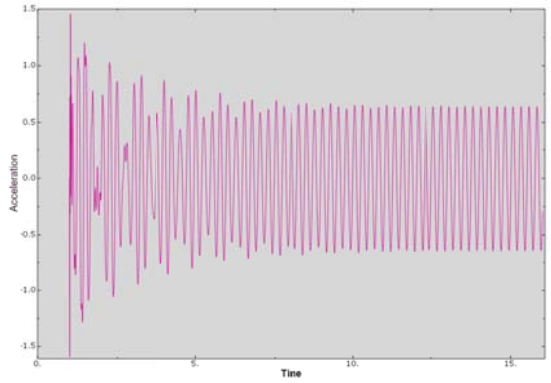

Figure (C.7) *Time increment = 0.005s, element size=0.2m.*

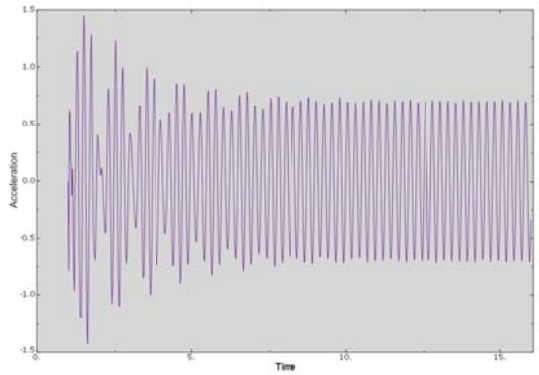

Figure (C.8) *Time increment = 0.01s, element size=0.2m.*

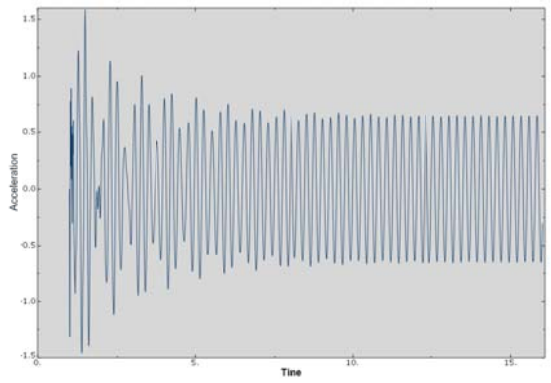

Figure (C.9) *Time increment = 0.02s, element size=0.2m.*

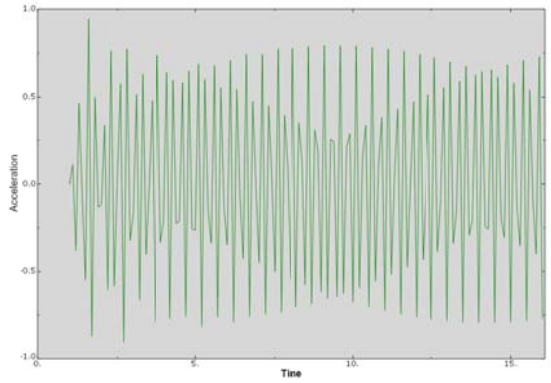

Figure (C.10) *Time increment = 0.1s, element size=0.2m.*

D APPENDIX D
STIFFNESS TRANSITION DEFINITIONS

The stiffness transition zone is defined by Figure (D.1).

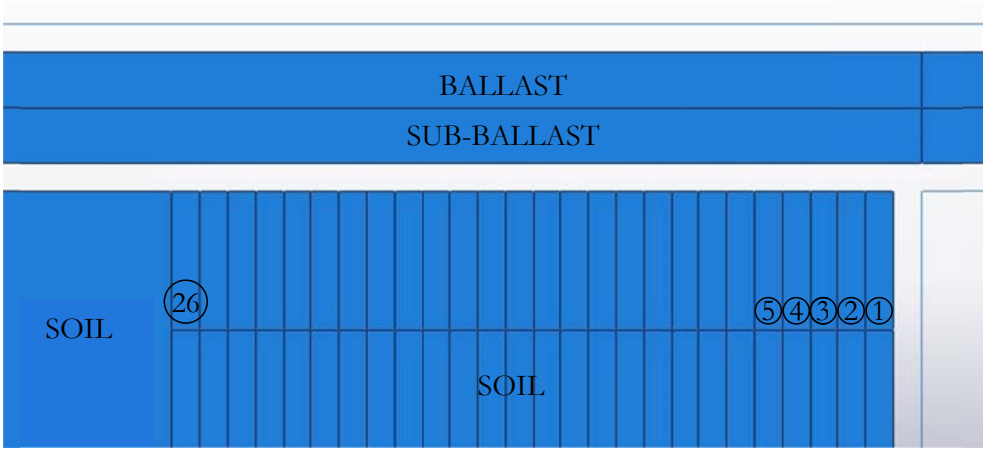

Figure (D.1) *Definition of transition zone.*

The used Young's modulus (1-26) of each run (1-13) of the parametric study is defined in a column of Table (D.1).

Table (D.1) *Stiffness transition definition, all values in GPa.*

	Run												
	1	2	3	4	5	6	7	8	9	10	11	12	13
E_1	10,00	30,00	10,00	30,00	20,00	20,00	20,00	20,00	10,00	10,00	30,00	30,00	20,00
E_2	9,51	28,51	9,51	28,51	18,58	19,24	18,58	19,24	9,30	9,62	27,87	28,85	19,01
E_3	9,02	27,02	9,02	27,02	17,17	18,47	17,17	18,47	8,60	9,24	25,74	27,71	18,02
E_4	8,53	25,53	8,53	25,53	15,75	17,71	15,75	17,71	7,89	8,87	23,61	26,56	17,03
E_5	8,03	24,03	8,03	24,03	14,33	16,95	14,33	16,95	7,19	8,49	21,48	25,41	16,03
E_6	7,54	22,54	7,54	22,54	12,92	16,19	12,92	16,19	6,49	8,11	19,35	24,26	15,04
E_7	7,05	21,05	7,05	21,05	11,50	15,42	11,50	15,42	5,79	7,73	17,21	23,12	14,05
E_8	6,56	19,56	6,56	19,56	10,08	14,66	10,08	14,66	5,08	7,35	15,08	21,97	13,06
E_9	6,07	18,07	6,07	18,07	8,67	13,90	8,67	13,90	4,38	6,97	12,95	20,82	12,07
E_{10}	5,58	16,58	5,58	16,58	7,25	13,14	7,25	13,14	3,68	6,60	10,82	19,67	11,08
E_{11}	5,08	15,08	5,08	15,08	5,83	12,37	5,83	12,37	2,98	6,22	8,69	18,53	10,08
E_{12}	4,59	13,59	4,59	13,59	4,42	11,61	4,42	11,61	2,27	5,84	6,56	17,38	9,09
E_{13}	4,10	12,10	4,10	12,10	3,00	10,85	3,00	10,85	1,57	5,46	4,43	16,23	8,10
E_{14}	3,61	10,61	3,61	10,61	1,58	10,08	1,58	10,08	0,87	5,08	2,30	15,08	7,11
E_{15}	3,12	9,12	3,12	9,12	0,17	9,32	0,17	9,32	0,17	4,71	0,17	13,94	6,12
E_{20}	2,63	7,63	2,63	7,63	0,17	8,56	0,17	8,56	0,17	4,33	0,17	12,79	5,13
E_{21}	2,13	6,13	2,13	6,13	0,17	7,80	0,17	7,80	0,17	3,95	0,17	11,64	4,13
E_{22}	1,64	4,64	1,64	4,64	0,17	7,03	0,17	7,03	0,17	3,57	0,17	10,49	3,14
E_{23}	1,15	3,15	1,15	3,15	0,17	6,27	0,17	6,27	0,17	3,19	0,17	9,35	2,15
E_{24}	0,66	1,66	0,66	1,66	0,17	5,51	0,17	5,51	0,17	2,81	0,17	8,20	1,16
E_{25}	0,17	0,17	0,17	0,17	0,17	4,74	0,17	4,74	0,17	2,44	0,17	7,05	0,17
E_{26}	0,17	0,17	0,17	0,17	0,17	3,98	0,17	3,98	0,17	2,06	0,17	5,90	0,17
E_{27}	0,17	0,17	0,17	0,17	0,17	3,22	0,17	3,22	0,17	1,68	0,17	4,76	0,17
E_{28}	0,17	0,17	0,17	0,17	0,17	2,46	0,17	2,46	0,17	1,30	0,17	3,61	0,17
E_{29}	0,17	0,17	0,17	0,17	0,17	1,69	0,17	1,69	0,17	0,92	0,17	2,46	0,17
E_{30}	0,17	0,17	0,17	0,17	0,17	0,93	0,17	0,93	0,17	0,55	0,17	1,31	0,17
soil	0,17	0,17	0,17	0,17	0,17	0,17	0,17	0,17	0,17	0,17	0,17	0,17	0,17

E APPENDIX E
REGRESSION ANALYSIS MATLAB SCRIPT

```
%%%%%%%%%%%%%%%%%%%%%%%%%%%%%%%%%%%%%%%%%%%%%%%%%%%%%%%%%%%%%%%%%%%%%%%%
% PREFORMING REGRESSION ANALYSIS ON BRIGADE OUTPUT %
% By: Peter Nilsson, 2010-10-22                    %
%%%%%%%%%%%%%%%%%%%%%%%%%%%%%%%%%%%%%%%%%%%%%%%%%%%%%%%%%%%%%%%%%%%%%%%%

clc
clear all
close all
format compact

[fname,cat]=uigetfile('*.rpt','Choose an input file');

X=load([cat fname]);
scr = [0 0 1280 800];

A=X(:,2:14);
U=X(:,15:27);
V=X(:,28:40);

%%%%% Substracting initial displacement
for i=1:13
    U(:,i)=U(:,i)-U(1,i);
end
%%%%%%%%%%%%%%%%%%%%%%%%%%%%%%%%%%%%%%%%%%%%%%%%%%%%%%%%%%%%%%%%%%%%%%%%

%%%%% Collecting extreme values
u=zeros(15,1); a=u; v=u;
for i=1:13
    u(i)=max(abs(U(:,i)));
    v(i)=max(abs(V(:,i)));
    a(i)=max(abs(A(:,i)));
end
u(14)=u(13); v(14)=v(13); a(14)=a(13);
```

```
u(15)=u(13); v(15)=v(13); a(15)=a(13);
%%%%%%%%%%%%%%%%%%%%%%%%%%%%%%%%
%%% PLOTS
x=1:15;
figure('position',scr)
subplot(2,2,1)
plot(x,u*1000,'o')
xlabel('attempt nr')
ylabel('maximum displacent [mm]')
title('B-B design')
subplot(2,2,2)
plot(x,v,'o')
xlabel('attempt nr')
ylabel('maximum velocity [m/s]')
title('B-B design')
subplot(2,2,3)
plot(x,a,'o')
ylabel('maximum acceleration [m/s2]')
xlabel('attempt nr')
title('B-B design')

%%%% SAVING THE PLOT
saveas(gcf,[cat '1'],'jpg')
%%%%%%%%%%%%%%%%%%%%%%%%%%

%%% Box-B matrix
bbd=zeros(15,9);
bbd(:,1:3)=bbdesign(3);
bbd(:,4)=bbd(:,1).*bbd(:,2);
bbd(:,5)=bbd(:,1).*bbd(:,3);
bbd(:,6)=bbd(:,2).*bbd(:,3);
bbd(:,7)=bbd(:,1).^2;
bbd(:,8)=bbd(:,2).^2;
bbd(:,9)=bbd(:,3).^2;
```

```
%%% solving system of equations
coeff_u=u\bbd;
coeff_v=v\bbd;
coeff_a=a\bbd;

%%% plotting results
xs=1:9;

%%% bar-plot
figure('position',scr)
subplot(2,2,1)
bar(xs,coeff_u)
title('displacement coeff B-B design')
axis([0 10 min(coeff_u) max(coeff_u)])
xlabel('coefficient nr')
subplot(2,2,2)
bar(xs,coeff_v)
title('velocity coeff B-B design')
axis([0 10 min(coeff_v) max(coeff_v)])
xlabel('coefficient nr')
subplot(2,2,3)
bar(xs,coeff_a)
title('acceleration coeff B-B design')
axis([0 10 min(coeff_a) max(coeff_a)])
xlabel('coefficient nr')

%%%% SAVING THE PLOT
saveas(gcf,[cat '2'],'jpg')
%%%%%%%%%%%%%%%%%%%%%%%%%

%%% normal plot
figure('position',scr)
subplot(2,2,1)
normplot(coeff_u)
title('displacement coeff B-B design')
subplot(2,2,2)
```

```
normplot(coeff_v)
title('velocity coeff B-B design')
subplot(2,2,3)
normplot(coeff_a)
title('acceleration coeff B-B design')

%%%% SAVING THE PLOT
saveas(gcf,[cat '3'],'jpg')
%%%%%%%%%%%%%%%%%%%%%%%%%%

close all

%%%%%%%%%%%%%%%%%%%%%%%%%%%%%%%%%%%%%%%%%%%%%%%%
%%%%%%%%%% REGRESSION ANALYSIS %%%%%%%%%%
%%%%%%%%%%%%%%%%%%%%%%%%%%%%%%%%%%%%%%%%%%%%%%%%

%%% creating the Box-B matrix with real values
bbd_reg=zeros(13,3);
r=bbdesign(3);
bbd_reg(:,1:3)=r(1:13,:);

for i=1:13
    if bbd_reg(i,1)==-1
    bbd_reg(i,1)=290;
    end
    if bbd_reg(i,1)==0
    bbd_reg(i,1)=310;
    end
    if bbd_reg(i,1)==1
    bbd_reg(i,1)=330;
    end
    if bbd_reg(i,2)==-1
    bbd_reg(i,2)=10;
    end
    if bbd_reg(i,2)==0
    bbd_reg(i,2)=20;
```

```
    end
    if bbd_reg(i,2)==1
    bbd_reg(i,2)=30;
    end
    if bbd_reg(i,3)==-1
    bbd_reg(i,3)=2.8;
    end
    if bbd_reg(i,3)==0
    bbd_reg(i,3)=4;
    end
    if bbd_reg(i,3)==1
    bbd_reg(i,3)=5.2;
    end
end

%%%
a=a(1:13);
u=u(1:13);
v=v(1:13);

%%% preforming regression analysis
var = {'beta','r','rsquare','tstat','standres','yhat'};

R2 = zeros(3,1);

%%%% acceleration
res_a = regstats(a,bbd_reg,'quadratic',var);
beta_a = res_a.beta;
r_a = res_a.r;
R2(3) = res_a.rsquare;
t_a = res_a.tstat;
pval_a = t_a.pval;
yhat_a = res_a.yhat;
st_res_a = res_a.standres;

%%%% displacement
```

```
res_u = regstats(u,bbd_reg,'quadratic',var);
beta_u = res_u.beta;
r_u = res_u.r;
R2(1) = res_u.rsquare;
t_u = res_u.tstat;
pval_u = t_u.pval;
yhat_u = res_u.yhat;
st_res_u = res_u.standres;

%%%% velocity
res_v = regstats(v,bbd_reg,'quadratic',var);
beta_v = res_v.beta;
r_v = res_v.r;
R2(2) = res_v.rsquare;
t_v = res_v.tstat;
pval_v = t_v.pval;
yhat_v = res_v.yhat;
st_res_v = res_v.standres;

R2

%%%%%% PLOTS

%%%%%% significance
xs=1:length(pval_u);
figure('position',scr)
subplot(2,2,1)
bar(xs,pval_u)
title('significance of coeff, u, full regr')
subplot(2,2,2)
bar(xs,pval_v)
title('significance of coeff, v, full regr')
subplot(2,2,3)
bar(xs,pval_a)
title('significance of coeff, a, full regr')
```

```
%%%% SAVING THE PLOT
saveas(gcf,[cat '4'],'jpg')
%%%%%%%%%%%%%%%%%%%%%%%%%%

%%%%%% regression coefficients
xs=2:length(beta_u);
figure('position',scr)
subplot(2,2,1)
bar(xs,beta_u(2:length(beta_u)))
title('displacement coeff. full regr')
subplot(2,2,2)
bar(xs,beta_v(2:length(beta_u)))
title('velocity coeff. full regr')
subplot(2,2,3)
bar(xs,beta_a(2:length(beta_u)))
title('acceleration coeff. full regr')

%%%% SAVING THE PLOT
saveas(gcf,[cat '5'],'jpg')
%%%%%%%%%%%%%%%%%%%%%%%%%%

%%%%% Residuals vs fits

figure('position',scr)
subplot(2,2,1)
plot(yhat_u,st_res_u,'o')
title('residuals vs. fits displ. full regr.')
subplot(2,2,2)
plot(yhat_v,st_res_v,'o')
title('residuals vs. fits vel. full regr')
subplot(2,2,3)
plot(yhat_a,st_res_a,'o')
title('residuals vs. fits acc. full regr')

%%%% SAVING THE PLOT
saveas(gcf,[cat '6'],'jpg')
```

```
%%%%%%%%%%%%%%%%%%%%%%%%%%

%%%%% Normplot of residuals

figure('position',scr)
subplot(2,2,1)
normplot(r_u)
title('displacement residual normplot full regr.')
subplot(2,2,2)
normplot(r_v)
title('velocity residual normplot full regr.')
subplot(2,2,3)
normplot(r_a)
title('acceleration residual normplot full regr.')

%%%% SAVING THE PLOT
saveas(gcf,[cat '7'],'jpg')
%%%%%%%%%%%%%%%%%%%%%%%%%%

%%%% regression coeff in normplot

figure('position',scr)
subplot(2,2,1)
normplot(beta_u(2:10))
title('displacement coeff. normplot full regr.')
subplot(2,2,2)
normplot(beta_v(2:10))
title('velocity coeff. normplot full regr.')
subplot(2,2,3)
normplot(beta_a(2:10))
title('acceleration residual normplot full regr.')

%%%% SAVING THE PLOT
saveas(gcf,[cat '15'],'jpg')
%%%%%%%%%%%%%%%%%%%%%%%%%%
```

```
close all


%%%%%%%%%%%%%%%%%%%%%%%%%%
%%%%% POST ANALYSIS %%%%%
%%%%%%%%%%%%%%%%%%%%%%%%%%

%%% preforming linear regression analysis on requested variables

%%% creating the full quadratic matrix

bbd_reg_post=[bbd_reg(:,1:3) bbd_reg(:,1).*bbd_reg(:,2)
bbd_reg(:,1).*bbd_reg(:,3) bbd_reg(:,2).*bbd_reg(:,3)
bbd_reg(:,1).^2 bbd_reg(:,2).^2 bbd_reg(:,3).^2];

signi = input('choose sign.-level for acceptance, 0-1   ');

X_u=zeros(9,1);
X_v=zeros(9,1);
X_a=zeros(9,1);
for i=2:length(X_u)
    if pval_u(i) < signi
        X_u(i-1)=1;
    end
    if pval_v(i) < signi
        X_v(i-1)=1;
    end
    if pval_a(i) < signi
        X_a(i-1)=1;
    end
end

pos=0;
bbd_reg_u=zeros(13,length(find(X_u)));
for i=1:length(X_u)
```

```
if X_u(i)==1
    bbd_reg_u(:,pos+1)=bbd_reg_post(:,i);
    pos=pos+1;
end
end

pos=0;
bbd_reg_v=zeros(13,length(find(X_v)));
for i=1:length(X_v)
if X_v(i)==1
    bbd_reg_v(:,pos+1)=bbd_reg_post(:,i);
    pos=pos+1;
end
end

pos=0;
bbd_reg_a=zeros(13,length(find(X_a)));
for i=1:length(X_a)
if X_a(i)==1
    bbd_reg_a(:,pos+1)=bbd_reg_post(:,i);
    pos=pos+1;
end
end


%%%% ACCELERATIONS

res_a = regstats(a,bbd_reg_a,'linear',var);
beta_a = res_a.beta;
r_a = res_a.r;
R2(3) = res_a.rsquare;
t_a = res_a.tstat;
pval_a = t_a.pval;
yhat_a = res_a.yhat;
st_res_a = res_a.standres;
```

```
%%%% DISPLACEMENTS

res_u = regstats(u,bbd_reg_u,'linear',var);
beta_u = res_u.beta;
r_u = res_u.r;
R2(1) = res_u.rsquare;
t_u = res_u.tstat;
pval_u = t_u.pval;
yhat_u = res_u.yhat;
st_res_u = res_u.standres;

%%%%% VELOCITYS

res_v = regstats(v,bbd_reg_v,'linear',var);
beta_v = res_v.beta;
r_v = res_v.r;
R2(2) = res_v.rsquare;
t_v = res_v.tstat;
pval_v = t_v.pval;
yhat_v = res_v.yhat;
st_res_v = res_v.standres;

%%%%%%%%%% PLOTS

R2

%%%%%%%%%% significance

xs_u=1:length(pval_u);
xs_v=1:length(pval_v);
xs_a=1:length(pval_a);

figure('position',scr)
subplot(2,2,1)
bar(xs_u,pval_u)
title('significance, u, mod. regr')
```

```
subplot(2,2,2)
bar(xs_v,pval_v)
title('significance, v, mod. regr')
subplot(2,2,3)
bar(xs_a,pval_a)
title('significance, a, mod. regr')

%%%% SAVING THE PLOT
saveas(gcf,[cat '8'],'jpg')
%%%%%%%%%%%%%%%%%%%%%%%%%%


%%%%%% regression coefficients
figure('position',scr)
subplot(2,2,1)
bar(xs_u,beta_u(1:length(beta_u)))
title('regression coefficients, u, mod. regr')
subplot(2,2,2)
bar(xs_v,beta_v(1:length(beta_v)))
title('regression coefficients, v, mod. regr')
subplot(2,2,3)
bar(xs_a,beta_a(1:length(beta_a)))
title('regression coefficients, a, mod. regr')

%%%% SAVING THE PLOT
saveas(gcf,[cat '9'],'jpg')
%%%%%%%%%%%%%%%%%%%%%%%%%%

%%%%% Residuals vs fits

figure('position',scr)
subplot(2,2,1)
plot(yhat_u,st_res_u,'o')
title('residuals vs. fits, u, mod. regr')
subplot(2,2,2)
plot(yhat_v,st_res_v,'o')
```

```
title('residuals vs. fits, v, mod. regr')
subplot(2,2,3)
plot(yhat_a,st_res_a,'o')
title('residuals vs. fits, a, mod. regr')

%%%% SAVING THE PLOT
saveas(gcf,[cat '10'],'jpg')
%%%%%%%%%%%%%%%%%%%%%%%%%%

%%%%% Normplot of residuals

figure('position',scr)
subplot(2,2,1)
normplot(r_u)
title('residual normplot, u, mod. regr')
subplot(2,2,2)
normplot(r_v)
title('residual normplot, v, mod. regr')
subplot(2,2,3)
normplot(r_a)
title('residual normplot, a, mod. regr')

%%%% SAVING THE PLOT
saveas(gcf,[cat '11'],'jpg')
%%%%%%%%%%%%%%%%%%%%%%%%%%

close all

%%%% REGRESSION FUNCTIONS

%%%% displacement

% matrix for L-variation
V=(max(bbd_reg(:,1))+min(bbd_reg(:,1)))/2;
E=(max(bbd_reg(:,2))+min(bbd_reg(:,2)))/2;
L=[min(bbd_reg(:,3)):0.01:max(bbd_reg(:,3))]';
```

```
Lvary=zeros(length(L),9);
Lvary(:,1)=V; Lvary(:,2)=E; Lvary(:,3)=L; Lvary(:,4)=V*E;
Lvary(:,5)=V*L;
Lvary(:,6)=E*L; Lvary(:,7)=V.^2; Lvary(:,8)=E.^2; Lvary(:,9)=L.^2;


%matrix for E-variation
V=(max(bbd_reg(:,1))+min(bbd_reg(:,1)))/2;
E=[min(bbd_reg(:,2)):0.01:max(bbd_reg(:,2))]';
L=(max(bbd_reg(:,3))+min(bbd_reg(:,3)))/2;
Evary=zeros(length(E),9);
Evary(:,1)=V; Evary(:,2)=E; Evary(:,3)=L; Evary(:,4)=V*E;
Evary(:,5)=V*L;
Evary(:,6)=E*L; Evary(:,7)=V.^2; Evary(:,8)=E.^2; Evary(:,9)=L.^2;


%matrix for V-variation
V=[min(bbd_reg(:,1)):0.01:max(bbd_reg(:,1))]';
E=(max(bbd_reg(:,2))+min(bbd_reg(:,2)))/2;
L=(max(bbd_reg(:,3))+min(bbd_reg(:,3)))/2;
Vvary=zeros(length(V),9);
Vvary(:,1)=V; Vvary(:,2)=E; Vvary(:,3)=L; Vvary(:,4)=V*E;
Vvary(:,5)=V*L;
Vvary(:,6)=E*L; Vvary(:,7)=V.^2; Vvary(:,8)=E.^2; Vvary(:,9)=L.^2;


u_valid=find(X_u);
v_valid=find(X_v);
a_valid=find(X_a);


u_Vvary_0=0;
for i=1:length(beta_u)
    if i==1
        u_Vvary=beta_u(i);
        u_Vvary_0=u_Vvary;
    else
    u_Vvary=beta_u(i)*Vvary(:,u_valid(i-1));
    u_Vvary=u_Vvary+u_Vvary_0;
    u_Vvary_0=u_Vvary;
end
```

```
end

u_Lvary_0=0;
for i=1:length(beta_u)
    if i==1
        u_Lvary=beta_u(i);
        u_Lvary_0=u_Lvary;
    else
    u_Lvary=beta_u(i)*Lvary(:,u_valid(i-1));
    u_Lvary=u_Lvary+u_Lvary_0;
    u_Lvary_0=u_Lvary;
end
end

u_Evary_0=0;
for i=1:length(beta_u)
    if i==1
        u_Evary=beta_u(i);
        u_Evary_0=u_Evary;
    else
    u_Evary=beta_u(i)*Evary(:,u_valid(i-1));
    u_Evary=u_Evary+u_Evary_0;
    u_Evary_0=u_Evary;
end
end

figure('position',scr)
subplot(2,2,1)
plot(Vvary(:,1),u_Vvary*1e3)
xlabel('v [km/h]')
ylabel('u [mm]')
subplot(2,2,2)
plot(Evary(:,2),u_Evary*1e3)
xlabel('E [GPa]')
ylabel('u [mm]')
subplot(2,2,3)
```

```
plot(Lvary(:,3),u_Lvary*1e3)
xlabel('L [m]')
ylabel('u [mm]')

%%%% SAVING THE PLOT
saveas(gcf,[cat '12'],'jpg')
%%%%%%%%%%%%%%%%%%%%%%%%%%

v_Vvary_0=0;
for i=1:length(beta_v)
    if i==1
        v_Vvary=beta_v(i);
        v_Vvary_0=v_Vvary;
    else
    v_Vvary=beta_v(i)*Vvary(:,v_valid(i-1));
    v_Vvary=v_Vvary+v_Vvary_0;
    v_Vvary_0=v_Vvary;
end
end

v_Lvary_0=0;
for i=1:length(beta_v)
    if i==1
        v_Lvary=beta_v(i);
        v_Lvary_0=v_Lvary;
    else
    v_Lvary=beta_v(i)*Lvary(:,v_valid(i-1));
    v_Lvary=v_Lvary+v_Lvary_0;
    v_Lvary_0=v_Lvary;
end
end

v_Evary_0=0;
for i=1:length(beta_v)
    if i==1
        v_Evary=beta_v(i);
```

```
        v_Evary_0=v_Evary;
    else
    v_Evary=beta_v(i)*Evary(:,v_valid(i-1));
    v_Evary=v_Evary+v_Evary_0;
    v_Evary_0=v_Evary;
end
end

figure('position',scr)
subplot(2,2,1)
plot(Vvary(:,1),v_Vvary)
xlabel('v [km/h]')
ylabel('v [m/s]')
subplot(2,2,2)
plot(Evary(:,2),v_Evary)
xlabel('E [GPa]')
ylabel('v [m/s]')
subplot(2,2,3)
plot(Lvary(:,3),v_Lvary)
xlabel('L [m]')
ylabel('v [m/s]')

%%%% SAVING THE PLOT
saveas(gcf,[cat '13'],'jpg')
%%%%%%%%%%%%%%%%%%%%%%%%%%%

a_Vvary_0=0;
for i=1:length(beta_a)
    if i==1
        a_Vvary=beta_a(i);
        a_Vvary_0=a_Vvary;
    else
    a_Vvary=beta_a(i)*Vvary(:,a_valid(i-1));
    a_Vvary=a_Vvary+a_Vvary_0;
    a_Vvary_0=a_Vvary;
end
```

```
end

a_Lvary_0=0;
for i=1:length(beta_a)
    if i==1
        a_Lvary=beta_a(i);
        a_Lvary_0=a_Lvary;
    else
    a_Lvary=beta_a(i)*Lvary(:,a_valid(i-1));
    a_Lvary=a_Lvary+a_Lvary_0;
    a_Lvary_0=a_Lvary;
end
end

a_Evary_0=0;
for i=1:length(beta_a)
    if i==1
        a_Evary=beta_a(i);
        a_Evary_0=a_Evary;
    else
    a_Evary=beta_a(i)*Evary(:,a_valid(i-1));
    a_Evary=a_Evary+a_Evary_0;
    a_Evary_0=a_Evary;
end
end

figure('position',scr)
subplot(2,2,1)
plot(Vvary(:,1),a_Vvary)
xlabel('v [km/h]')
ylabel('a [m/s2]')
subplot(2,2,2)
plot(Evary(:,2),a_Evary)
xlabel('E [GPa]')
ylabel('a [m/s2]')
subplot(2,2,3)
```

```
plot(Lvary(:,3),a_Lvary)
xlabel('L [m]')
ylabel('a [m/s2]')

%%%% SAVING THE PLOT
saveas(gcf,[cat '14'],'jpg')
%%%%%%%%%%%%%%%%%%%%%%%%%%

close all
```

F APPENDIX F

TRANSITION ZONE DEFINITIONS OF EACH RUN IN LENGTH STUDY.

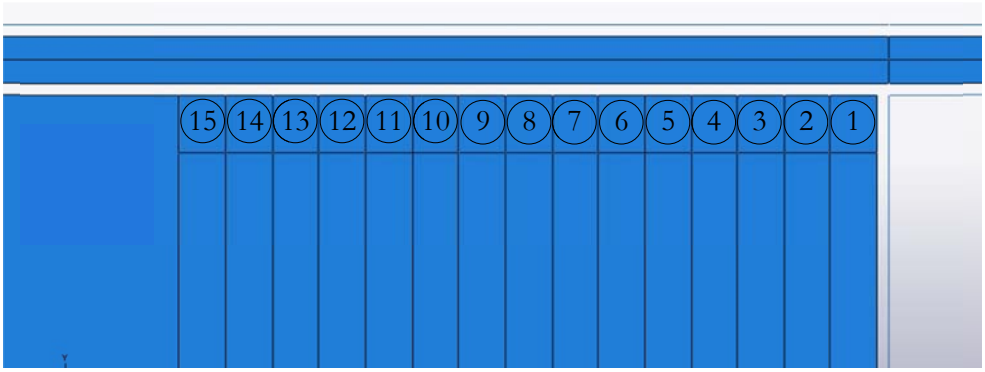

Figure (F.1) *Transition zone schematic.*

Table (F.1) *Transition zone definitions of each run.*

	Run														
	1,0	2,0	3,0	4,0	5,0	6,0	7,0	8,0	9,0	10,0	11,0	12,0	13,0	14,0	15,0
E_1	30,0	30,0	30,0	30,0	30,0	30,0	30,0	30,0	30,0	30,0	30,0	30,0	30,0	30,0	30,0
E_2	0,2	15,1	20,1	22,5	24,0	25,0	25,7	26,3	26,7	27,0	27,3	27,5	27,7	27,9	28,0
E_3		0,2	10,1	15,1	18,1	20,1	21,5	22,5	23,4	24,0	24,6	25,0	25,4	25,7	26,0
E_4			0,2	7,6	12,1	15,1	17,2	18,8	20,1	21,1	21,9	22,5	23,1	23,6	24,0
E_5				0,2	6,1	10,1	13,0	15,1	16,7	18,1	19,2	20,1	20,8	21,5	22,0
E_6					0,2	5,1	8,7	11,4	13,4	15,1	16,4	17,6	18,5	19,3	20,1
E_7						0,2	4,4	7,6	10,1	12,1	13,7	15,1	16,2	17,2	18,1
E_8							0,2	3,9	6,8	9,1	11,0	12,6	13,9	15,1	16,1
E_9								0,2	3,5	6,1	8,3	10,1	11,6	13,0	14,1
E_{10}									0,2	3,2	5,6	7,6	9,3	10,8	12,1
E_{11}										0,2	2,9	5,1	7,1	8,7	10,1
E_{12}											0,2	2,7	4,8	6,6	8,1
E_{13}												0,2	2,5	4,4	6,1
E_{14}													0,2	2,3	4,1
E_{15}														0,2	2,2
soil	0,2	0,2	0,2	0,2	0,2	0,2	0,2	0,2	0,2	0,2	0,2	0,2	0,2	0,2	0,2

G APPENDIX G
PSD PLOT SCRIPT

```
%%%%%%%% READING BRIGADE ACC. SIGNAL OUTPUT %%%%%%%%%%

clear all
close all
clc

X1=load('d:\skolan\kurser\examensarbete\matlab\frekvenssvep\ram.rp
t');
X2=load('d:\skolan\kurser\examensarbete\matlab\frekvenssvep\0.rpt'
);
X3=load('d:\skolan\kurser\examensarbete\matlab\frekvenssvep\stiff.
rpt');

t1=X1(:,1);  %time vector for frame alone
a1=X1(:,2);  %acc. signal of the frame alone

t2=X2(:,1);  %time signal for full models
a2=X2(:,2);  %acc. signal, full model, no stiffness transition
a3=X3(:,2);  %acc. signal of full model, stiffest transition zone

NFFT_1 = length(t1);            %FFT-length of frame alone
Fs_1 = length(a1)/max(t1);      %sampling freq. of frame alone

NFFT_2 = length(t2);            %FFT-length of full models
Fs_2 = length(a2)/max(t2);      %sampling freq. of full model


[Pxx_a1,f1] = pwelch(a1,hanning(NFFT_1),0,NFFT_1,Fs_1);
[Pxx_a2,f2] = pwelch(a2,hanning(NFFT_2),0,NFFT_2,Fs_2);
[Pxx_a3,f3] = pwelch(a3,hanning(NFFT_2),0,NFFT_2,Fs_2);

%%% Plotting PSDs
```

```
figure
semilogy(f1,Pxx_a1)%plot(f1,Pxx_a1)
axis([0 30 0 max(Pxx_a1)])
xlabel('\fontsize{12}frequency [Hz]')
ylabel('\fontsize{12}PSD')

figure
semilogy(f2,Pxx_a2)%plot(f2,Pxx_a2)
axis([0 30 0 max(Pxx_a2)])
xlabel('\fontsize{12}frequency [Hz]')
ylabel('\fontsize{12}PSD')

figure
semilogy(f3,Pxx_a3)%plot(f3,Pxx_a3)
axis([0 30 0 max(Pxx_a3)])
xlabel('\fontsize{12}frequency [Hz]')
ylabel('\fontsize{12}PSD')


%%% Plotting acc. signal
figure
plot(t1,a1)
xlabel('\fontsize{12}time [s]')
ylabel('\fontsize{12}acceleration [m/s^2]')

figure
plot(t2,a2)
xlabel('\fontsize{12}time [s]')
ylabel('\fontsize{12}acceleration [m/s^2]')

figure
plot(t2,a3)
xlabel('\fontsize{12}time [s]')
ylabel('\fontsize{12}acceleration [m/s^2]')
```